# Decay of correlations in fluids: The one-component plasma from Debye-Hückel to the asymptotic-high-density limit

R. J. F. Leote de Carvalho,[1,2] R. Evans,[1] and Y. Rosenfeld[1,3]
[1]*H. H. Wills Physics Laboratory, University of Bristol, Royal Fort, Tyndall Avenue, Bristol BS8 1TL, United Kingdom*
[2]*Ecole Normale Supérieure de Lyon, Laboratoire de Physique, 46, Allée d'Italie, 69364 Lyon Cedex 07, France*
[3]*Physics Department, Nuclear Research Center Negev, P.O. Box 9001, Beer-Sheva 84190, Israel*
(Received 9 September 1998)

The decay of structural correlations in the classical one-component plasma is analyzed by calculating the poles of the Fourier transform of the total (pairwise) correlation function $h(r)$ for two integral equation theories, the soft mean spherical approximation and the hypernetted chain (HNC). We show that for all except the largest values of the plasma coupling constant $\Gamma$, the leading-order pole contribution provides an accurate description of $h(r)$ at intermediate range, as well as the ultimate asymptotic decay. The crossover from monotonic decay at weak coupling to exponentially damped oscillatory decay at strong coupling is shown to arise from the same mechanism as that which occurs for charge correlations in binary ionic fluids. We calculate the values of $\Gamma$ at which the crossover occurs in the two theories. The role of higher-order poles and (within the HNC) other singularities in determining the intermediate range behavior of $h(r)$ for strong coupling is discussed. We investigate the properties of the solutions of the integral equations in the strong coupling, $\Gamma \rightarrow \infty$, asymptotic high-density limit (AHDL). Padé approximants are employed in order to test the validity of the scaling laws proposed for the potential energy, direct correlation function, and for the poles and their contributions to $h(r)$ in the AHDL. Our numerical results provide strong support for the validity of the theoretical predictions concerning the AHDL. [S1063-651X(99)01002-8]

PACS number(s): 61.20.Ne, 61.20.Gy, 64.10.+h, 52.25.−b

## I. INTRODUCTION

The one-component plasma (OCP) can be regarded as the simplest model of an ionic fluid. It describes classical point ions, of charge $e$, interacting via the Coulomb potential $e^2/r$ and immersed in a uniform neutralizing background of charge. In spite of its simplicity, the OCP plays a key role in the physics of dense stellar material [1] and as a reference fluid for determining the properties of certain liquid metals, the effects of electron screening being treated perturbatively [2]. The statistical mechanics of the OCP are well studied. Indeed near equal effort has been expended in determining the properties of the OCP [1] as for those of the hard-sphere fluid, which serves as the primary reference system for simple fluids where the interatomic potentials are short-ranged [2]. An important feature of the OCP is that its equilibrium properties depend on a single dimensionless parameter, the plasma coupling constant

$$\Gamma \equiv \beta \frac{e^2}{a_{\mathrm{WS}}}, \tag{1}$$

where $\beta \equiv (k_B T)^{-1}$, $k_B$ is Boltzmann's constant, $T$ is the temperature, and $a_{\mathrm{WS}}$ is the Wigner-Seitz or ion-sphere radius, which in three dimensions (3D) is

$$a_{\mathrm{WS}} \equiv (3/4\pi\rho)^{1/3} \tag{2}$$

with $\rho$ being the number density of the ions. All the standard integral equation theories of liquids and many of the more recent descendants have been applied to the OCP and their regime of validity has been ascertained by comparison with the extensive computer simulation studies which exist for this model [1]. The structure and thermodynamic properties are well-described by Debye-Hückel theory in the weak-coupling regime $\Gamma \ll 1$. At high couplings the hypernetted-chain (HNC) approximation has proved the most successful of the standard theories and is accurate for a wide range of $\Gamma$: $0.05 \leqslant \Gamma \leqslant 50$ [3]. For larger values of $\Gamma$, the HNC yields radial distribution functions $g(r)$ with less pronounced maxima than the corresponding Monte Carlo results [4,1]. Better agreement is achieved by resorting to MHNC (modified HNC) approximations but these retain the main features of the original HNC [5]. In a remarkable early paper, Ng [4] showed that the HNC could be solved numerically, giving stable solutions, for $\Gamma$ up to 7000 or thereabouts. This is particularly striking when one notes that the Monte Carlo simulations predict a freezing transition in the OCP for $\Gamma \sim 178$ [6,7]. In other words, solutions of the HNC exist for $\Gamma$ well into the metastable fluid region. Ng [4] also showed that the decay of $g(r)-1 \equiv h(r)$, in the range $10 \leqslant r/a_{\mathrm{WS}} \leqslant 20$, could be fitted by a single (exponentially damped) sinusoidal function [see Eq. (41)] for $200 \leqslant \Gamma \leqslant 7000$. Such a result implies that at longer and intermediate range, pairwise correlations are governed by a dominant conjugate pair of complex poles in $\hat{h}(q)$, the Fourier transform of $h(r)$. This observation provided some of the motivation for the present study, which analyzes the decay of pairwise correlations for the full range of $\Gamma$, i.e., from the weak-coupling, Debye-Hückel regime where $h(r)$ exhibits monotonic (exponential) decay to the very strong-coupling, $\Gamma \rightarrow \infty$, limit.

In order to investigate correlations in the OCP, we employ and, where necessary, improve upon methods developed in our earlier studies of the asymptotics of correlation functions [8–11]. We focus on two integral equation approaches, namely (i) the HNC, which, like its more sophisticated relatives, can only be solved numerically so that the determina-

 

tion of the poles of $\hat{h}(q)$ is rather demanding, and (ii) the SMSA (soft mean spherical approximation) [12], which has the advantage of providing an analytical solution for the OCP while still yielding reasonable results for structure and for thermodynamic properties; $g(r)$ can take on negative values in the SMSA but only for large couplings, i.e., $\Gamma \gtrsim 400$. Although these two theories appear to have very different origins, at strong coupling they share several common features [13–15]. This was ascertained by studying their thermodynamic properties, as related to the closure relations which define the two approximations. In particular, the variational free-energy functionals of the pair functions are very similar. Such considerations lead to investigations of the AHDL (asymptotic high-density limit), defined as the strong-coupling limit $\Gamma \to \infty$, in which the compressibility vanishes. It was established [13–15] that the HNC and SMSA for soft-core potentials, together with the variational perturbation theory [based on the PY (Percus-Yevick) treatment of the hard-sphere reference fluid], become identical in the AHDL. In this limit the theories have the same Madelung energy, which is an exact lower bound to the true potential energy, and the pair direct correlation functions can be given a simple meaning, i.e., as overlap volumes for hard-core fluids and as *interactions* between *smeared particles* for soft potentials. More significantly for the present work, it is conjectured that for a certain wide class of potentials, the poles of $\hat{h}(q)$ should exhibit some universal features in the approach to the AHDL. These features are summarized in Sec. II C but the main result is that in the AHDL the poles in the OCP should be identical to those arising from the PY treatment of hard spheres in the limit where the packing fraction $\eta = 1$, which once again corresponds to the vanishing of the compressibility. In an earlier paper [14] by one of us, the AHDL of the OCP was investigated using the SMSA and Ng's [4] numerical solutions for the HNC. Here we readdress this limit by performing new calculations and using the methods of pole analysis developed in [8–11]. In addition, we carry out Padé analysis on data from both the HNC and SMSA calculations to examine the possible scaling behavior of various quantities in the approach to the AHDL. This enables us to test further the earlier conjectures and to ascertain what (large) values of $\Gamma$ are required before the properties of the OCP are those characteristic of the AHDL, i.e., when scaling behavior, with the small parameter $\varepsilon = 1 - \eta(\Gamma)$, is appropriate. Although one can associate an *ideal liquid* with the limit $\eta = 1$ and imagine performing some perturbative expansion in $\varepsilon$ to describe the properties of dense liquids, it is not obvious that such a procedure should work. Recall that $\eta = 1$ lies well beyond the close-packing limit $\eta = 0.74$ for hard spheres.

The universality associated with the AHDL does not extend to intermediate values of $\Gamma$. Unlike the hard-sphere fluid, where only conjugate pairs of complex poles arise and $h(r)$ is always oscillatory, the OCP develops a pair of pure imaginary poles at some particular value of $\Gamma$, here designated by $\Gamma_K$, and for $\Gamma < \Gamma_K$ the ultimate decay of $h(r)$ is monotonic (exponential). Several attempts have been made to determine $\Gamma_K$, using theory and simulation [1], and this quantity was expected to lie between about 1 and 3. However, the precise mechanism leading to the onset of oscillations in $h(r)$ has remained somewhat obscure. Here we show that the mechanism is the same as that which determines the onset of charge oscillations in a binary ionic fluid (electrolyte) [10], described first by Kirkwood [16]. We provide accurate estimates of $\Gamma_K$ within the HNC and the SMSA.

Our paper is organized as follows. In Sec. II we summarize the relevant integral equation theories and describe the theory for the asymptotic decay of pair correlations in the OCP. Prescriptions are given for determining the poles of $\hat{h}(q)$ and their contributions to $h(r)$ in both the HNC and SMSA. The possible role of singularities other than simple poles is discussed. Section II C contains a brief account of the properties of the OCP in the AHDL. In Sec. III we describe the results of our calculations, comparing our results for the leading-order pole with those obtained by Ng [4] in his fitting procedure. We show that the leading-order pole contribution in both the HNC and SMSA provides an accurate account of $h(r)$ for separations $r$ down to second nearest neighbors (not just asymptotically), provided $\Gamma \lesssim 1500$, attesting to the usefulness of the pole expansion. While the procedures we have developed for calculating the poles work well at leading order, there are severe difficulties in determining higher-order poles. Section III B discusses how spurious poles may be generated from numerical solutions of the HNC and other integral equation theories, pointing out that some earlier publications have probably reported such spurious poles, believing these to be genuine. In Sec. III C we consider second- (next-to-leading-) order contributions to $h(r)$. We show that in the case of the SMSA the contribution from the next-to-leading-order conjugate pair of poles leads to a splitting of the second maximum in $h(r)$ for very large values of $\Gamma$. Similar splittings are found in the HNC but we argue that these are likely to be associated (primarily) with other singularities, i.e., logarithmic branch points which should arise in this approximation. Section III D describes the trajectories of the OCP poles in the complex plane as a function of $\Gamma$, comparing the results with those for the hard-sphere fluid as a function of $\eta$. Finally, in Sec. III E we focus on the results of our Padé analysis of structural properties and the potential energy in the AHDL. We make some concluding remarks in Sec. IV.

## II. THEORY

### A. Summary of integral equation theory of liquids

The standard approach to the static properties of liquids [2] is based upon the Ornstein-Zernike (OZ) integral equation, which for a homogeneous one-component fluid reads

$$h(r) = c(r) + \rho \int d\mathbf{r}' h(|\mathbf{r} - \mathbf{r}'|) c(|\mathbf{r}|'), \tag{3}$$

where $\mathbf{r}$ is the position vector. This equation defines the *direct correlation function*, $c(r)$, in terms of the total correlation function, $h(r)$, which is in turn related to the radial distribution function, $g(r)$, by $h(r) = g(r) - 1$. In Fourier space the OZ equation takes the simple form

$$\hat{h}(q) = \frac{\hat{c}(q)}{1 - \rho \hat{c}(q)}. \tag{4}$$

Here $\hat{f}(q)$ denotes the 3D Fourier transform of a spherically symmetric function $f(r)$, i.e.,

$$\hat{f}(q)=4\pi\int_0^\infty dr\ r^2 f(r)\frac{\sin(qr)}{qr},$$
$$f(r)=\frac{1}{2\pi^2}\int_0^\infty dq\ q^2\hat{f}(q)\frac{\sin(qr)}{qr}. \tag{5}$$

It can be shown using diagrammatic analysis [2] that for a system characterized by a pairwise interaction potential $\phi(r)$ the exact closure to the OZ equation is

$$h(r)+1=e^{-\beta\phi(r)+h(r)-c(r)-b(r)}, \tag{6}$$

where $-b(r)$ is the *bridge* function, the sum of all *bridge* or *elementary* diagrams.

The HNC closure to the OZ relation simply sets the bridge function in Eq. (6) to zero at all distances, i.e., $b_{\mathrm{HNC}}(r)\equiv 0$. This closure can be conveniently written as

$$c(r)+\beta\phi(r)=g(r)-1-\ln g(r)\geqslant 0. \tag{7}$$

For a specified potential $\phi(r)$ the HNC can be solved numerically using an iterative procedure [2].

The HNC plays a pivotal role in developing other closure approximations to the OZ relation. If the bridge function $-b(r)$ were known, one could determine the *exact* statistical mechanics by solving the HNC for the *effective* potential $\phi^{\mathrm{eff}}(r)=\phi(r)+\beta^{-1}b(r)$. Although $b(r)$ is not known *exactly*, it has been argued [5] that this function carries *universal* features which are determined by the bridge function for hard spheres. In the MHNC approach the HNC equation is solved for an effective potential $\phi^{\mathrm{eff}}(r)$ which employs the hard-sphere bridge function calculated with a suitably chosen hard-sphere diameter.

The MSA (mean spherical approximation) is a closure to the OZ relation designed for systems with a hard-core repulsion, i.e., $\phi(r)=\infty$ for $r<d$, where $d$ is the hard-core diameter. This closure reads

$$g(r)=0,\quad r<d\quad\text{and}\quad c(r)+\beta\phi(r)=0,\quad r>d, \tag{8}$$

where the first equation is an exact result and the second constitutes the approximation. The MSA also implies a specific choice of bridge function, namely $b_{\mathrm{MSA}}(r)=g(r)-1-\ln g(r)$ for $r>d$. The functions $g(r)$ and $c(r)$ in the MSA are discontinuous at $r=d$. In the case of soft-core potentials such as the OCP, one can choose a particular hard-core diameter, $R$, so that the MSA gives

$$g(r=R^+)=0, \tag{9}$$

i.e., $g(r)$ can be forced to be continuous (although its first derivative will still be discontinuous at $r=R$) through careful choice of the hard-core diameter. The condition (9) can be used together with Eq. (8), with $d=R$, to define the SMSA closure, an extension of the MSA to soft-core potentials. Clearly $R$ is an effective hard-core diameter and the resulting $g(r)$ can be regarded as an acceptable solution to the MSA for the soft potential.

### B. Asymptotic decay of correlations

The theory for the OCP outlined below follows closely the analysis made for the asymptotic decay of correlations presented in [8] for simple fluids and in [10] for ionic fluids.

Outside the critical region, the ultimate decay of the direct correlation function of a simple fluid at large distances $r$ is given by $c(r)\rightarrow-\beta\phi(r)$, which in the case of the OCP translates into $c(r)\rightarrow-\beta e^2/r$. It is therefore convenient to define a short-ranged direct correlation function, $c^{sr}(r)$, by subtracting the long-ranged Coulomb decay

$$c^{sr}(r)\equiv c(r)+\frac{\beta e^2}{r}. \tag{10}$$

The Fourier transform of $c(r)$ is then

$$\rho\hat{c}(q)=\rho\hat{c}^{sr}(q)-\frac{\kappa_D^2}{q^2}, \tag{11}$$

where $\kappa_D^2\equiv 4\pi\rho\Gamma a_{\mathrm{WS}}$. $\kappa_D$ is the inverse Debye screening length. We assume that $c^{sr}(r)$ is exponentially decaying so that its Fourier transform $\hat{c}^{sr}(q)$ has only even powers in the Taylor expansion about $q=0$,

$$\hat{c}^{sr}(q)=c^{(0)}+c^{(2)}q^2+c^{(4)}q^4+c^{(6)}q^6+\cdots. \tag{12}$$

Consequently, $\hat{c}(q)$ and $\hat{h}(q)$ are even and we can write

$$h(r)=\frac{1}{2\pi^2 r}\int_0^\infty dq\ q\ \sin(qr)\hat{h}(q)$$
$$=\frac{1}{4\pi^2 ri}\int_{-\infty}^{\infty}dq\ qe^{iqr}\frac{\hat{c}(q)}{1-\rho\hat{c}(q)}. \tag{13}$$

Any poles at complex $q=\alpha_1+i\alpha_0$ are then given by the zeros of the denominator,

$$1-\rho\hat{c}(q)=1-\rho\hat{c}^{sr}(q)+\frac{\kappa_D^2}{q^2}=0. \tag{14}$$

The integral in Eq. (13) can be carried out by contour integration. If no singularities other than simple poles exist, then choosing an infinite radius semicircle in the upper half-plane, we obtain

$$h(r)=\sum_n A_n\frac{e^{iq_n r}}{r}\quad\text{with}\quad A_n\equiv-\frac{q_n}{2\pi\rho^2(d\hat{c}(q)/dq)_{q_n}}, \tag{15}$$

where the operator $d/dq$ represents the derivative with respect to the variable $q$ and $q_n$ is the $n$th pole.

From Eq. (15) it is straightforward to see that the ultimate decay of $h(r)$ should be driven by the pole or poles closest to the real axis (smallest $\alpha_0$). If this pole is pure imaginary, i.e., if $q_n=i\alpha_0$, then the leading decay is determined by

$$h(r)\sim A\frac{e^{-\alpha_0 r}}{r}. \tag{16}$$

In turn, if the pole closest to the real axis is the complex number $q_n=\alpha_1+i\tilde{\alpha}_0$, then it follows that $-\alpha_1+i\tilde{\alpha}_0$ is also a solution of Eq. (14) and the ultimate decay of $h(r)$, determined by the conjugate pair of complex poles $\pm\alpha_1+i\tilde{\alpha}_0$, is

$$h(r)\sim|\tilde{A}|\frac{e^{-\tilde{\alpha}_0 r}}{r}(e^{i(\alpha_1 r-\theta)}+e^{-i(\alpha_1 r-\theta)})$$

$$\sim 2|\tilde{A}|\frac{e^{-\tilde{\alpha}_0 r}}{r}\cos(\alpha_1 r-\theta), \tag{17}$$

where we have used the fact that the amplitudes of the $+$ and $-$ poles, $A^{\pm}\equiv|A^{\pm}|e^{\mp i\theta^{\pm}}$, have the same modulus, $|A^{+}|=|A^{-}|\equiv|\tilde{A}|$, and their phases satisfy $\theta^{+}=-\theta^{-}\equiv\theta$.

Within the MSA we expect the only singularities to be an infinite number of simple poles. However, in other approximations such as the HNC other singularities are indeed present. The HNC closure determines the decay of the direct correlation function to be

$$c(r)\sim-\beta\phi(r)+\frac{1}{2}h^2(r)+\cdots \tag{18}$$

which follows by expanding the right-hand side of Eq. (7). Therefore one expects $c^{sr}(r)\sim\lambda(r)$ with $\lambda(r)\equiv\frac{1}{2}h^2(r)$. If the pole closest to the real axis is a pure imaginary pole $i\alpha_0$, then the asymptotic decay of the total correlation function is given by Eq. (16). Hence $\lambda(r)\sim A^2e^{-2\alpha_0}/2r^2$. This behavior is associated with logarithmic branch point singularities of $\hat{\lambda}(q)$ at $q=\pm 2i\alpha_0$, namely

$$\hat{\lambda}(q)\sim i\frac{1}{2}\frac{2\pi A^2}{q}\ln\frac{1-iq/2\alpha_0}{1+iq/2\alpha_0}. \tag{19}$$

The right-hand side of Eq. (19) is simply the Fourier transform of $A^2e^{-2\alpha_0}/2r^2$. It immediately follows that $\hat{c}(q)$ must have these branch points too. Moreover, from the occurrence of $\hat{c}(q)$ in the denominator of the OZ relation

$$1+\rho\hat{h}(q)=\frac{1}{1-\rho\hat{c}(q)}, \tag{20}$$

one expects $\hat{h}(q)$ to have branch points at $q=\pm 2i\alpha_0$ also. This singularity leads to another term in the asymptotic expansion of $h(r)$,

$$h(r)\sim A\frac{e^{-\alpha_0 r}}{r}+A^2F(r)\frac{e^{-2\alpha_0 r}}{r^2}, \tag{21}$$

where $F(r)$ is a function that vanishes like $1/\ln^2 r$ as $r\to\infty$. This function can be obtained explicitly by contour integration around the branch cut in the upper complex half-plane. Since $F(r)$ vanishes like $1/\ln^2(r)$, the second term on the right-hand side of Eq. (21) should be much smaller than the first except at short and, perhaps, intermediate range.

The argument can be generalized to all the (complex) poles $q_n$ of $\hat{h}(q)$ and the expansion of $h(r)$ then becomes

$$h(r)=\sum_n A_n\frac{e^{iq_n r}}{r}+\sum_n A_n^2F_n(r)\frac{e^{i2q_n r}}{r^2}. \tag{22}$$

Further details of the derivation of $F_n(r)$ can be found in [17] where a similar discussion was given for the HNC treatment of binary ionic fluids.

#### *1. Poles in the SMSA*

In Appendix A we give the analytical solution to the SMSA for the OCP as obtained from the MSA treatment of the system of charged hard spheres immersed in an oppositely charged continuum background. The explicit expression for $\hat{c}(q)$ can be obtained from the analytical solution for $c(r)$ and this was given by Rosenfeld [14]. The correct expression for $\hat{c}(q)$ for the charged hard-sphere system in the MSA reads

$$\frac{\rho\hat{c}(q')}{24\eta}=\frac{A}{(q')^3}[\sin q'-q'\cos q']$$

$$+\frac{\kappa^2}{6(q')^5}\{[3(q')^2-6]\sin q'-[(q')^2-6]q'\cos q'\}+\frac{6\eta M^2}{(q')^4}\{2q'\sin q'-[(q')^2-2]\cos q'-2\}$$

$$+\frac{\eta}{2(q')^6}(A+\kappa^2V)\{[4(q')^2-24]q'\sin q'-[(q')^4-12(q')^2+24]\cos q'+24\}$$

$$+\frac{\eta\kappa^2}{60(q')^2}\{[6(q')^4-120(q')^2+720]q'\sin q'-[(q')^6-30(q')^4+360(q')^2-720]\cos q'-720\}$$

$$-\frac{\Gamma}{(q')^2}\cos q', \tag{23}$$

where $q' \equiv qR$. Equation (23) corrects Eq. (C8) in [14] which contains two misprints. For the OCP in the SMSA, the expression (23) holds with $M \equiv 0$ and the effective hard-sphere diameter $R$ is determined by solving Eq. (A9) for the packing fraction $\eta(\Gamma)$. $\kappa^2 = 12\Gamma\eta^{2/3}$ and the quantities $A$ and $V$ are functions of $\eta$ defined in Appendix A. In order to find the poles of $\hat{h}(q)$, we must solve the transcendental equation $1-\rho\hat{c}(q)=0$ for $q=\alpha_1+i\alpha_0$. This can be achieved by deriving equations for the real and imaginary parts of $1-\rho\hat{c}(q)$ and then solving the resulting two equations for $\alpha_0$ and $\alpha_1$ using a Newton-Raphson procedure.

The amplitudes $A_n$ entering the pole expansion (15) require only the derivative $d\hat{c}(q)/dq$. For a pure imaginary pole, the derivative is readily evaluated analytically using Eq. (23). For complex poles, the numerical evaluation of the amplitudes and phases can be carried out using complex algebra, avoiding the need to separate imaginary and real parts in the analytical expression for the derivative $d\hat{c}(q)/dq$.

#### *2. Poles in the HNC*

The HNC for the OCP must be solved numerically using an iterative procedure. We have used an efficient code which is based upon Gillan's method [18]. The Coulomb potential is separated from $c(r)$ in the standard way and is added back at the end of the calculation.

Below, we give a prescription for calculating the poles of the OCP based on the approach developed in [8] for simple fluids with short-ranged potentials. As we shall see, this method is useful for calculating the leading-order pole(s) but has limited use for determining the higher-order poles of the OCP in the HNC approximation since the integrals which are involved for the latter do not always converge. With the exception of Ref. [17] this limitation has not been realized fully in previous works [8,11,19–22] where equivalent prescriptions for calculating the poles for short-ranged potentials and for ionic fluids were given. We shall return to this point later.

The poles $q=\alpha_1+i\alpha_0$ are the complex solutions of Eq. (14), which can be rewritten in the more convenient form

$$1+\frac{\kappa_D^2}{q^2}=4\pi\rho\int_0^\infty dr\; r^2 c^{sr}(r)\frac{\sin(qr)}{qr}. \tag{24}$$

By separating imaginary and real parts, we obtain the following two equations:

$$\alpha_0\left(1-\frac{\kappa_D^2}{\alpha_0^2+\alpha_1^2}\right)=4\pi\rho\int_0^\infty dr\; rc^{sr}(r)\sinh(\alpha_0 r)\cos(\alpha_1 r), \tag{25}$$

$$\alpha_1\left(1+\frac{\kappa_D^2}{\alpha_0^2+\alpha_1^2}\right)=4\pi\rho\int_0^\infty dr\; rc^{sr}(r)\cosh(\alpha_0 r)\sin(\alpha_1 r) \tag{26}$$

which are equivalent to Eqs. (4a) and (4b) in [8] for the poles in simple fluids with short-ranged potentials. This pair of equations can be solved numerically for $\alpha_0$ and $\alpha_1$ using a Newton-Raphson procedure with $c^{sr}(r)$ as input. However, note that the integrals in these equations might not always converge. Assume, for example, that the leading pole is pure imaginary, given by $q=i\alpha_0$. Then, from the analysis carried out in Sec. II B [see Eq. (16)], the ultimate decay of $h(r)$ is $\sim Ae^{-\alpha_0 r}/r$. Within the HNC closure the decay of the direct correlation function is given by Eq. (18) so that the short-ranged direct correlation function decays as

$$c^{sr}(r)\sim\frac{1}{2}A^2\frac{e^{-2\alpha_0 r}}{r^2}. \tag{27}$$

It follows that the integrals in Eqs. (25) and (26) should diverge for any pole whose imaginary part is larger than $2\alpha_0$. We arrive at the same conclusion if the decay of $h(r)$ is controlled by a conjugate pair of complex poles. In general, the integrals in Eqs. (25) and (26) converge only for complex $q$ such that $\mathrm{Im}[q]\lesssim 2\alpha_0$, where $\alpha_0$ is the imaginary part of the leading pole(s). In practice (see Sec. III) all the other poles lie outside the convergence range and Eqs. (25) and (26) allow us to determine the leading-order pole(s) only.

Pure imaginary poles $q=i\alpha_0$ are determined by Eq. (25) alone, with $\alpha_1 \equiv 0$. This equation then simplifies to

$$1-\left(\frac{\kappa_D}{\alpha_0}\right)^2=4\pi\rho\int_0^\infty dr\; rc^{sr}(r)\frac{\sinh(\alpha_0 r)}{\alpha_0}. \tag{28}$$

For fluids with short-ranged potentials the imaginary poles satisfy the same equation but with $\kappa_D \equiv 0$ and $c^{sr}(r)$ replaced by $c(r)$. It was shown in [8] that for such fluids there is at most one imaginary pole. This is no longer the case in the OCP. The presence of the Coulomb term $-(\kappa_D/q)^2$ in $\hat{c}(q)$ modifies the analysis. In fact, as we discuss later in Sec. III A, we find that Eq. (28) has two solutions in the weak coupling regime (small $\Gamma$) and none at strong coupling (large $\Gamma$).

In Appendix B we give a prescription for evaluating the amplitude and phase of contributions to $h(r)$ arising from simple poles.

### C. Asymptotic high-density properties of the HNC integral equation

Here we summarize some general properties of the HNC and other integral equations in the asymptotic high-density limit (AHDL), i.e., the limit in which the compressibility vanishes. As mentioned earlier, exact liquid state theory for pair correlations functions can be reduced to an HNC equation for some (effective) potential. Thus the properties of the solution of this equation for different potentials are of central importance. For pairwise potentials $\phi(r)$ with strong repulsion at short distances, the AHDL solution of the HNC equation has *universal* features [15,14], some of which are listed below. We use the Wigner-Seitz radius $a_{\mathrm{WS}}$ as the unit of length, i.e., $r' \equiv r/a_{\mathrm{WS}}$, and provide specific examples for the OCP in 3D. Further details are given in the original papers [15,14].

(i) The Madelung energy is an exact lower bound for the potential energy $U$. This Madelung energy is the sum of the self-energies of individual dressed particles (Onsager *atoms*) and for the OCP in 3D,

$$\beta\frac{U}{N}=\beta u_{\mathrm{OA}}=-\frac{9}{10}\Gamma, \tag{29}$$

where $u_{\mathrm{OA}}$ is the self-energy of an Onsager *atom* consisting of a point charge at the center of a neutralizing unit sphere having the background charge density. It is equal to the energy integral with a universal pair correlation function,

$$\beta\frac{U}{N}\equiv\frac{1}{2}\rho\int\beta\phi(r)[g(r)-1]d^D\mathbf{r}$$

$$=\frac{1}{2}\Omega_D^{-1}\int\beta\phi(r')[g_D(r')-1]d^D\mathbf{r}', \tag{30}$$

where $\beta\phi(r')\equiv\Gamma/r'$ for the OCP and $\Omega_D$ is the volume of a unit $D$-dimensional sphere. The universal functions $g_D(r)$ denote the limit $\eta\to1$ of the solution of the PY equation for $D$-dimensional hard spheres of packing fraction $\eta$.

(ii) In the AHDL the direct correlation function of the OCP in 3D is given by

$$-\frac{c(r')}{\Gamma}=\Psi(r')$$

$$=\frac{6}{5}-\frac{1}{2}(r')^2+\frac{3}{16}(r')^3-\frac{1}{160}(r')^5,\quad r'\leqslant2$$

$$=\frac{1}{r'},\quad r'>2, \tag{31}$$

where $\Psi(r')$ is the electrostatic interaction between two spheres with the Wigner-Seitz radius where the charge is smeared uniformly inside the sphere. It follows that in the AHDL,

$$-\frac{c(r=0)}{\Gamma}=\frac{6}{5}. \tag{32}$$

(iii) In the AHDL the properties of the HNC equation mimic those of the MSA. The HNC builds an ion sphere automatically in this limit. In particular, the pair exclusion condition $g(r')=0,\ r'\leqslant2$ and the MSA condition $c(r')+\beta\Phi(r')=0,\ r'\geqslant2$ are satisfied. The AHDL corresponds to an effective packing fraction $\eta=1$, i.e., the solutions correspond to a hard-core diameter $R^{\infty}=2a_{\mathrm{WS}}$.

(iv) For the general class of Green's-function potentials, including the OCP and the screened Coulomb (Yukawa) fluid, the zeros of the Fourier transform of the direct correlation function, $\hat{c}(q)$, are universal in the AHDL. Let $\Omega(r)$ denote the overlap volume of two $D$-dimensional unit spheres whose centers are separated by a distance $r$ so that $\Omega(0)=\Omega_D$. Defining $\omega(r)=\Omega(r)/\Omega(0)$, then in 3D

$$\omega(r')=1-\frac{3}{4}r'+\frac{1}{16}(r')^3,\quad r'\leqslant2$$

$$=0,\quad r'>2. \tag{33}$$

The zeros of $\hat{c}(q)$ are identical to those of $\hat{\omega}(q)$ and the latter are given as the solutions $q_i'$ of

$$q'=\tan q' \tag{34}$$

with $q'=qa_{\mathrm{WS}}$. For the OCP in the AHDL, $\hat{c}(q)\propto-\Gamma\hat{\omega}(q)/q^2$ with similar relations for other potentials and the poles of $\hat{h}(q)$ [determined by the zeros of $1-\rho\hat{c}(q)$] are given by the zeros of $\hat{c}(q)$ in the limit $\Gamma\to\infty$. Thus, in the AHDL the poles of $\hat{h}(q)$ should take universal values given by the solutions of Eq. (34), i.e., the poles are real with the leading one given by

$$q_1'\equiv\alpha_1^{\infty}a_{\mathrm{WS}}=4.493\,409\,458\ldots\ . \tag{35}$$

Note that for hard spheres in the PY approximation one can show explicitly [14] that in the AHDL ($\eta=1$) the poles of $\hat{h}(q)$ are given by solutions of Eq. (34) with $q'=qa_{\mathrm{WS}}=qd/(2\eta^{1/3})$, where $d$ is the hard-sphere diameter.

(v) The approach to the AHDL is quantified by the small parameter

$$\varepsilon\equiv1-\eta. \tag{36}$$

In the SMSA treatment of the OCP, $\eta(\Gamma)$ is determined by solving Eq. (A9), while in the HNC a prescription is required for the effective diameter $R$ which determines $\eta=(R/2a_{\mathrm{WS}})^3$. We return to this later.

Scaling relations (expansions in powers of $\varepsilon$) have been proposed for the behavior of the poles and their amplitudes [14]. For soft potentials, e.g., the OCP, the imaginary ($\tilde{\alpha}_0$) and real ($\alpha_1$) parts of the leading pole are expected to obey the relations

$$\tilde{\alpha}_0a_{\mathrm{WS}}=A_{\tilde{\alpha}_0}\varepsilon^6+\cdots \tag{37}$$

and

$$\alpha_1a_{\mathrm{WS}}=\alpha_1^{\infty}a_{\mathrm{WS}}-A_{\alpha_1}\varepsilon^3+\cdots \tag{38}$$

in 3D. Note that the powers depend on the dimensionality only, but the amplitudes $A_{\tilde{\alpha}_0}$ and $A_{\alpha_1}$ are not universal and need not be the same for different theories. (The higher poles have equivalent expansions [14].) The amplitude $|\tilde{A}|$ of the leading pole contribution to $h(r)$ [see Eq. (17)] also has a series expansion,

$$2\frac{|\tilde{A}|}{a_{\mathrm{WS}}}=2\frac{|\tilde{A}^{\infty}|}{a_{\mathrm{WS}}}+A_{\tilde{A}}\varepsilon^3+\cdots, \tag{39}$$

where

$$2\frac{|\tilde{A}^{\infty}|}{a_{\mathrm{WS}}}\equiv\frac{2}{3}\left(\frac{1+(\alpha_1^{\infty}a_{\mathrm{WS}})^2}{\alpha_1^{\infty}a_{\mathrm{WS}}}\right)=3.143\,971\,74\ldots \tag{40}$$

is universal but $A_{\tilde{A}}$ is not.

The analytical solution of the SMSA for the OCP is consistent with Eqs. (37)–(40). However, the general analysis [14] which leads to these results, along with that for the internal energy (29) and for $c(r=0)$ (32), is not completely rigorous in the mathematical sense and it is of considerable interest to test these conjectures for the HNC and other theories. Indeed this is one of the aims of our present study.

TABLE I. Leading conjugate pair of complex poles $\pm\alpha_1+i\tilde{\alpha}_0$ and the respective amplitudes $|\tilde{A}|$ and phases $\varphi\equiv-\theta+\pi/2$ for the OCP treated in the HNC for different values of $\Gamma$; (a) as obtained from the pole analysis prescribed in Sec. II B 2; (b) Ng's results for the parameters as listed in Table III of [4], obtained from fitting the asymptote (41) to his numerical data for $h(r)$ in the range $10\leqslant r/a_{\mathrm{WS}}\leqslant 20$.

| | $\tilde{\alpha}_0 a_{\mathrm{WS}}$ | | $\alpha_1 a_{\mathrm{WS}}$ | | $2\lvert\tilde{A}\rvert/a_{\mathrm{WS}}$ | | $\varphi\equiv-\theta+\pi/2$ | |
|---|---|---|---|---|---|---|---|---|
| $\Gamma$ | (a) | (b) | (a) | (b) | (a) | (b) | (a) | (b) |
| 200 | 0.4255 | 0.4251 | 4.1637 | 4.1638 | 2.8902 | 2.8714 | 0.4656 | 0.4641 |
| 250 | 0.3741 | 0.3736 | 4.1849 | 4.1851 | 2.8503 | 2.8226 | 0.4231 | 0.4195 |
| 300 | 0.3358 | 0.3352 | 4.2012 | 4.2013 | 2.8210 | 2.7878 | 0.3889 | 0.3859 |
| 350 | 0.3060 | 0.3053 | 4.2141 | 4.2143 | 2.8014 | 2.7627 | 0.3628 | 0.3596 |

## III. RESULTS OF CALCULATIONS

In this section we describe the results of our numerical calculations for structural properties of the OCP obtained using both the HNC and SMSA.

### A. Asymptotic decay of $h(r)$

We consider first the ultimate decay of $h(r)$ in the OCP. Ng [4] analyzed this problem in the framework of the HNC. Following a similar path to what we presented in Sec. II B, he argued (in our notation) that for sufficiently large $\Gamma$,

$$h(r)\sim 2|\tilde{A}|\frac{e^{-\tilde{\alpha}_0 r}}{r}\sin(\alpha_1 r+\varphi). \tag{41}$$

Comparison with Eq. (17) shows $\varphi\equiv-\theta+\pi/2$. However, Ng does not provide a means for calculating the poles of $\hat{h}(q)$, nor does he give the amplitude and the phase. In the weak coupling regime, $\Gamma\ll 1$, by expanding $\hat{c}(q)$ about $q=0$, he arrives at

$$\rho\hat{h}(q)\approx-\frac{3\Gamma}{3\Gamma+q^2a_{\mathrm{WS}}^2}, \tag{42}$$

which exhibits a simple pole at $qa_{\mathrm{WS}}=i(3\Gamma)^{1/2}=i\kappa_D a_{\mathrm{WS}}$. Thus

$$\rho h(r)\approx-\Gamma a_{\mathrm{WS}}\frac{e^{-\kappa_D r}}{r},\quad r\to\infty, \tag{43}$$

which is the Debye-Hückel asymptotic form valid only in the limit of very weak coupling [23,3].

For $\Gamma\gg 1$, Ng argues that the leading pole should be complex. For the range $200\leqslant\Gamma\leqslant 7000$, he fits the parameters $\tilde{\alpha}_0$, $\alpha_1$, $|\tilde{A}|$, and $\varphi$ in the asymptote (41) to the decay of the solution $h(r)$, obtained by solving numerically the HNC, calculated in the range $10\leqslant r/a_{\mathrm{WS}}\leqslant 20$.

Here we use the prescription described in Sec. II B 2 and Appendix B to compute the leading poles of $\hat{h}(q)$, their amplitudes, and phases for the OCP treated in the HNC. In Table I we compare our results with those of Ng, who fitted his numerical data to Eq. (41), and we find an excellent agreement. This means that the asymptote (41) provides a very accurate account of the decay of $h(r)$ over the range of distances used by Ng in his fitting analysis. As we shall see below, for this range of $\Gamma$, i.e., $200\leqslant\Gamma\leqslant 350$, the asymptote is also very accurate at much smaller distances.

The poles of the SMSA can be computed, in turn, using the prescription given in Sec. II B 1. At low $\Gamma$, in both the SMSA and the HNC, we find that the ultimate decay of $h(r)$ is given by a simple pole lying on the imaginary axis, $q=i\alpha_0$, as was expected. This leading pole is accompanied, however, by another imaginary pole, $i\alpha_0'$, with $\alpha_0'>\alpha_0$. As $\Gamma$ is increased, these two poles move towards each other and coalesce when a certain value of $\Gamma$ is reached. For consistency with previous work [10,24] we designate this particular value of $\Gamma$ the Kirkwood coupling, $\Gamma_K$. As $\Gamma$ is increased above $\Gamma_K$, the two poles move off the imaginary axis and symmetrically into the complex plane, giving rise to oscillatory decay of $h(r)$. This type of mechanism for the onset of oscillations in $h(r)$ for the OCP was alluded to by Choquard and Sari [25] and earlier by Del-Rio and DeWitt [26], but a full description was not given. As $\Gamma\to\Gamma_K^-$, the amplitudes of the two imaginary poles diverge. The amplitude of the pole closer to the real axis, $A$, is negative while the other, $A'$, is positive. Both amplitudes tend to equal absolute values as $\alpha_0\to\alpha_0'$ so that the combination

$$h(r)\sim A\frac{e^{-\alpha_0 r}}{r}+A'\frac{e^{-\alpha_0' r}}{r} \tag{44}$$

remains finite at $\Gamma_K$. For $\Gamma\gg\Gamma_K$, $h(r)$ decays as

$$h(r)\sim 2|\tilde{A}|\frac{e^{-\tilde{\alpha}_0 r}}{r}\cos(\alpha_1 r-\theta). \tag{45}$$

As $\Gamma\to\Gamma_K^+$, $|\tilde{A}|$ diverges but the phase $\theta\to-\pi/2$ and $\alpha_1\to 0^+$ (the complex poles coincide) so that $\cos(\alpha_1 r-\theta)\to 0$ and again $h(r)$ remains finite.

This scenario for the onset of oscillations in the OCP is identical to that found for the charge correlations in the restricted primitive model (RPM) [10,19]. It was first described by Kirkwood [16] in his discussion of the potential of mean force in strong electrolytes. It is also found in the Yukawa screened-RPM (YRPM) [24], a model similar to the RPM where screening is explicitly included by replacing the long-ranged Coulomb interactions by Yukawa potentials.

We have calculated $\Gamma_K$ in the SMSA and in the HNC. In the SMSA the two imaginary poles coalesce at $qa_{\mathrm{WS}}=i4.548$ when $\Gamma_K=2.1199$, and in the HNC at $qa_{\mathrm{WS}}=i2.85$ when $\Gamma_K=1.120$. Choquard and Sari [25] obtained

TABLE II. (a) The pair of imaginary poles $i\alpha_0$ and $i\alpha_0'$ and their respective amplitudes $A$ and $A'$, as obtained from the SMSA and HNC, are given for $\Gamma=1$. (b) The leading conjugate pair of complex poles $\pm\alpha_1+i\tilde{\alpha}_0$ and their respective amplitudes $|\tilde{A}|$ and phases $\theta$, as obtained from the SMSA and HNC, are given for three values of $\Gamma$. The poles of the HNC cannot be computed accurately at $\Gamma=7000$ using our prescription (see text). (c) The next-to-leading-order poles for the SMSA are given at two different values of $\Gamma$.

(a)

| | $\alpha_0 a_{WS}$ | | $A/a_{WS}$ | | $\alpha_0' a_{WS}$ | | $A'/a_{WS}$ | |
|---|---|---|---|---|---|---|---|---|
| $\Gamma$ | SMSA | HNC | SMSA | HNC | SMSA | HNC | SMSA | HNC |
| 1 | 1.8531 | 2.2457 | −1.3185 | −3.9219 | 13.492 | 3.3203 | 32.438 | 5.4343 |

(b)

| | $\tilde{\alpha}_0 a_{WS}$ | | $\alpha_1 a_{WS}$ | | $2\lvert\tilde{A}\rvert/a_{WS}$ | | $\theta$ | |
|---|---|---|---|---|---|---|---|---|
| $\Gamma$ | SMSA | HNC | SMSA | HNC | SMSA | HNC | SMSA | HNC |
| 10 | 1.9214 | 1.8099 | 3.6965 | 3.4677 | 5.3876 | 4.4748 | 0.2310 | 0.1729 |
| 100 | 0.6112 | 0.6201 | 4.0927 | 4.0864 | 3.0411 | 3.0625 | 0.9585 | 0.9507 |
| 7000 | 0.0340 | | 4.4043 | | 2.9050 | | 1.5204 | |

(c)

| $\Gamma$ | $\bar{\alpha}_0 a_{WS}$ | $\bar{\alpha}_1 a_{WS}$ | $2\lvert\bar{A}\rvert/a_{WS}$ | $\bar{\theta}$ |
|---|---|---|---|---|
| 100 | 2.2624 | 8.0631 | 8.4274 | 1.0053 |
| 7000 | 0.3948 | 7.4618 | 5.0732 | 1.3397 |

$\Gamma_K=1.0$ in the HNC from an analysis of Eq. (14). In numerical work, based on a modification of the HNC, Cooper [27] found that oscillations develop for $\Gamma$ between 2 and 3, and the same estimate was obtained by Hansen [7] from his Monte Carlo study. In an earlier study, Del-Rio and DeWitt [26] obtained $\Gamma_K=1.812$ and this is close to the value of 1.818 found by Deutsch *et al.* [28] from a graphical analysis. $\Gamma_K$ was also estimated to be approximately 1.0 in Appendix B of [5].

In Table II we compare the leading poles for the OCP as obtained from the SMSA and HNC for three values of $\Gamma$. The results from these two approaches are somewhat different in the weak coupling regime, $\Gamma\lesssim 1$, where the details of the approximation become important. At high $\Gamma$ the leading poles from the two theories become much closer. In Fig. 1(a) we compare the full $h(r)$ obtained from the SMSA and HNC at $\Gamma=1$ with the asymptotic contribution given by Eq. (44), i.e., that determined by the two imaginary poles in Table II. In the SMSA the agreement is remarkably good at all distances outside the imposed hard core. In the HNC the agreement is equally good down to about $r/a_{WS}\approx 1$. In Figs. 1(b) and 1(c) we plot the full $h(r)$ against the asymptote (45) obtained from the leading conjugate pair of complex poles as given in Table II. In Fig. 1(b), $\Gamma=10$ while in Fig. 1(c), $\Gamma=100$. The asymptotes obtained from the leading poles in the SMSA and HNC are almost identical for $\Gamma=100$, which is not surprising since the poles and the amplitudes obtained from the two theories are very close. In both the SMSA and the HNC, $h(r)$ is described accurately by the contribution from the leading conjugate pair of poles for distances down to about the second maximum. For a wide range of $\Gamma$, other (higher) poles and singularities do not play a role at intermediate and long range. Even the shorter range behavior is described in a sensible, qualitative fashion. As we shall discuss in Sec. III C, this scenario changes for $\Gamma\gtrsim 1500$, where other contributions become important.

### B. Spurious poles

In Sec. II B 2 we gave a prescription for calculating the poles of $\hat{h}(q)$ for the OCP treated in the HNC that should yield at least the leading-order pole(s). If the imaginary part of the leading pole(s) is $\alpha_0$ and the short-ranged direct correlation function decays like $c^{sr}(r)\sim\frac{1}{2}h^2(r)$, Eqs. (25) and (26) will diverge for any higher pole whose imaginary part $\gtrsim 2\alpha_0$. However, in the numerical evaluation of the integrals in this pair of equations, one is forced to truncate $c^{sr}(r)$ at some finite distance where the value of this function is *suitably* small. This may seem harmless at first sight but in fact it has important repercussions for the numerical solutions to Eqs. (25) and (26). Although the integrals should no longer converge, the truncation means that the numerical algorithm still converges. The issue is then how to separate the actual poles from any spurious solutions arising from truncation. In Fig. 2 we show the numerical solutions, at three different values of $\Gamma$, which we obtain from solving Eqs. (25) and (26) for $\alpha_0$ and $\alpha_1$ taking $c^{sr}(r)$ to be truncated beyond a distance $r$, chosen so that $c^{sr}(r)<1.5\times 10^{-9}$. The leading poles are given in Table II but for each $\Gamma$ we have found also a line of solutions with imaginary values at about $2\alpha_0$, with $\alpha_0$ the imaginary part of the leading pole(s). These values are in the region where convergence problems should arise.

In order to investigate whether the solutions constituting this line are actual poles or spurious solutions to Eqs. (25) and (26), we performed a simple test. We considered the hard-core Yukawa fluid

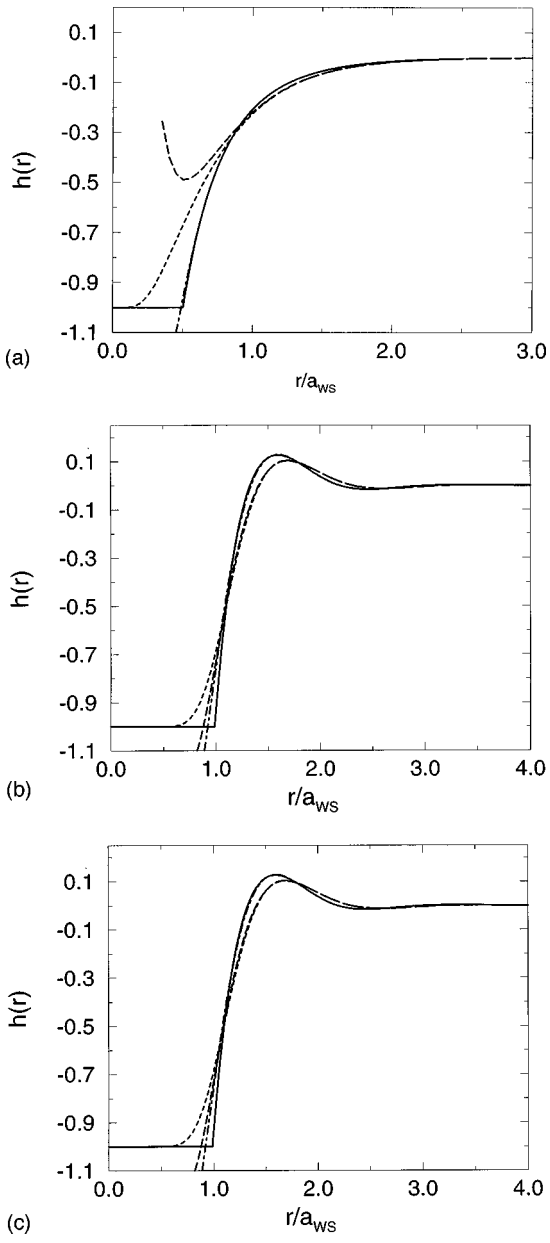


FIG. 1. Total correlation function $h(r)$ for the OCP treated in the SMSA (solid line) and HNC (dotted line), at three different values of $\Gamma$. In (a) $\Gamma=1$, in (b) $\Gamma=10$, and in (c) $\Gamma=100$. The dot-dashed line and the dashed line are the asymptotes in the SMSA and HNC, respectively. In (a) the decay is monotonic and the asymptote is given in Eq. (44). In (b) and (c) the ultimate decay is oscillatory and the asymptote is given in Eq. (45). The parameters of the asymptotes are given in Table II.

$$\phi_{\mathrm{Yuk}}(x)=\infty, \quad x\leqslant 1$$
$$=-\frac{De^{-\tilde{z}x}}{x}, \quad x>1, \tag{46}$$

where $x\equiv r/d$ and $d$ is the hard-sphere diameter. $D$ and $\tilde{z}$ are both positive constants. Brown *et al.* [29] have investigated the pole structure of $\hat{h}(q)$ for this model fluid treated in the MSA, which can be solved analytically (see [30] and also [31]). For consistency with their study, we take $D=\frac{9}{8}\epsilon e^{\tilde{z}}/(\frac{1}{3}+\tilde{z}^{-1}+\tilde{z}^{-2})$, where $\epsilon$ is an energy parameter.

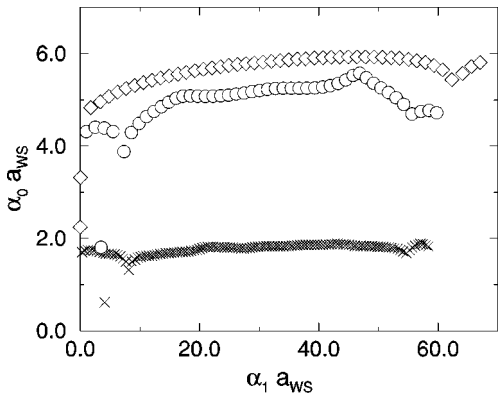


FIG. 2. Solutions of Eqs. (25) and (26) for the poles of the OCP treated in the HNC, at three different values of $\Gamma$. Only the right-hand complex pole $+\alpha_1+i\tilde{\alpha}_0$ is shown. $\diamond$ corresponds to $\Gamma=1$, $\bigcirc$ to $\Gamma=10$, and $\times$ to $\Gamma=100$. Note that for $\Gamma=1$ there are two poles lying on the imaginary axis. For $\Gamma=10$ the leading pole, with $\tilde{\alpha}_0\approx 1.8$, is well separated from the other solutions. For $\Gamma=100$ the leading pole, with $\tilde{\alpha}_0\approx 0.6$, is also well separated from the other solutions. The lines of closely spaced solutions, which extend to higher values of $\alpha_1$, are not actual poles but are spurious solutions arising from truncation of $c^{sr}(r)$.

Since $c(r)$ and its Fourier transform $\hat{c}(q)$ are known analytically, the poles can be calculated in a similar way to that described earlier for the SMSA, i.e., by separating the equation $1-\rho\hat{c}(q)=0$ into its imaginary and real parts and solving the two resulting equations for $\alpha_0$ and $\alpha_1$. This procedure enables us to find all the poles. Alternatively, we can attempt to use the method described by Evans *et al.* [8]. This is equivalent to that prescribed here for the HNC and (4a) and (4b) in [8] suffer from the same convergence problems as our Eqs. (25) and (26) in Sec. II B 2. In the MSA for the hard-core Yukawa fluid we have $c(r)\propto\exp(-\tilde{z}r)/r$ outside the hard core; the integrals in (4a) and (4b) in [8] diverge when the imaginary part of the pole is greater than $\tilde{z}$. Consequently, one can easily examine the range of convergence of the integrals simply by changing $\tilde{z}$ in the model. In Figs. 3(a) and 3(b) we show the poles of $\hat{h}(q)$ for the hard-core Yukawa fluid treated in the MSA, at a reduced temperature $T^*\equiv k_BT/\epsilon=1.18$ and reduced density $\rho^*\equiv\rho d^3=0.814$, as obtained from the analytical path and from solving Eqs. (4a) and (4b) in [8]. For $\tilde{z}=1$ [Fig. 3(a)] a line of spurious solutions is found at $\alpha_0 d\approx\tilde{z}$ when this latter method is employed. The leading conjugate pair of poles as obtained from both the analytical path and from (4a) and (4b) in [8] lies at $qd=\pm 6.63+i0.82$, i.e., $\alpha_0 d<1$. In this case the next-to-leading-order pole near $qd=\pm 12.4+i2.1$ (obtained from the analytical path) could not be found using the second method. For $\tilde{z}=2.5$ [Fig. 3(b)], and identical temperature and density, the leading pole shifts to $qd=\pm 6.69+i0.78$. Now, both the analytical path and the numerical solution of (4a) and (4b) of [8] yield not only this solution but also the next-to-leading-order conjugate pair of complex poles at $qd=\pm 12.53+i2.00$. Note that the imaginary part is still below $\tilde{z}=2.5$.

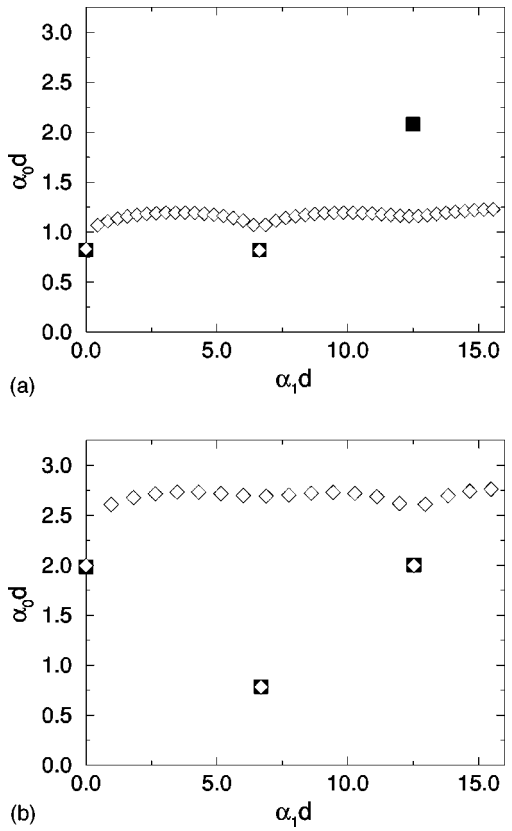


FIG. 3. The poles of the hard-core Yukawa fluid treated in the MSA for (a) $\tilde{z}=1$ and (b) $\tilde{z}=2.5$. The filled squares are the actual poles obtained by solving $1-\rho\hat{c}(q)=0$, using the analytical expression for $\hat{c}(q)$. The diamonds are the numerical solutions to Eqs. (4a) and (4b) in [8] (see text). The lines of diamonds extending to higher values of $\alpha_1$ in both (a) and (b) are not actual poles but correspond to spurious solutions.

An imaginary pole can be found using both methods and this lies at $qd=i1.99$, which is again below $\tilde{z}=2.5$. Equations (4a) and (4b) of [8] yield a line of spurious solutions at $\alpha_0 d\approx 2.5$, i.e., close to the value of $\tilde{z}$. Clearly this line is located where convergence problems are expected and the third pole obtained from the analytical path, which has $\alpha_0 d > \tilde{z}=2.5$, cannot be found. Given the strong similarity between the lines of solutions in Fig. 3 and those in Fig. 2, we conclude that the latter, for the OCP treated in the HNC, are a numerical artifact of our truncation.

These results suggest that the lines of *poles* in Fig. 1 of [11], for a truncated Lennard-Jones 6-12 fluid treated in the HNC and HMSA, are also spurious. In the HNC this line lies at about $3\alpha_0$, where $\alpha_0$ is the imaginary part of the leading poles, and this falls in the region of the complex plane where convergence problems are expected. In [20] a similar line of solutions was found, using identical equations for the poles, for the hard-sphere fluid treated in the HNC, and within another approximation that also leads to convergence problems. We believe these lines also correspond to spurious solutions. Similar numerical prescriptions for determining the poles of simple and ionic fluids from integral equation theories have been given [17,19,22]. These will also suffer from convergence problems.

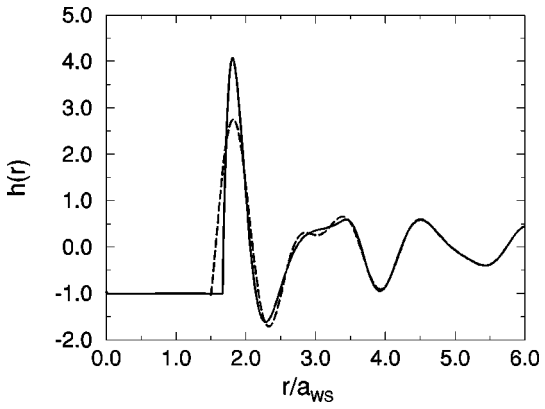


FIG. 4. Total correlation function $h(r)$ for the OCP treated in the SMSA at $\Gamma=7000$. The solid line is the solution to the integral equation while the dashed line is $h^a(r)$, obtained by adding the contribution from the leading and the next-to-leading conjugate pair of complex poles as given by Eq. (49). The parameters are given in Table II. Note that $g(r)=1+h(r)$ can take on negative values in this approximation.

### C. Second-order contributions to $h(r)$

If we subtract the ultimate asymptotic decay (45) from $h(r)$, then at sufficiently high $\Gamma$, i.e., $\Gamma>\Gamma_K$, we obtain the function

$$\overline{h}(r)\equiv h(r)-2|\tilde{A}|\frac{e^{-\tilde{\alpha}_0 r}}{r}\cos(\alpha_1 r-\theta). \tag{47}$$

Since the only singularities in the SMSA are simple poles and all contributions from conjugate pairs of complex poles to $h(r)$ in the expansion (15) have the same form, we expect $\overline{h}(r)$ to decay as

$$\overline{h}(r)\to 2|\overline{A}|\frac{e^{-\overline{\alpha}_0 r}}{r}\cos(\overline{\alpha}_1 r-\overline{\theta}),\quad r\to\infty, \tag{48}$$

i.e., as the contribution from the next-to-leading-order conjugate pair of poles, $q\equiv\pm\overline{\alpha}_1+i\overline{\alpha}_0$. The amplitude $|\overline{A}|$ and phase $\overline{\theta}$ are determined in a similar fashion to those for the leading-order pair of poles (see Sec. II B 2).

In his early study, Ng [4] noted the appearance of a shoulder in the second peak of the distribution function for the OCP treated in the HNC, when $\Gamma\gtrsim 1500$. He remarked that the shapes of the peaks at such strong coupling were unlike those found for simple fluids. Of course, we should recall that the OCP freezes into a bcc solid at about $\Gamma\approx 178$ [6,7] and therefore these unusual features develop deep in the metastable fluid region. The shoulder observed by Ng is not unique to the HNC. We found the SMSA solution also exhibits a split second peak in $h(r)$. In Fig. 4 we plot the SMSA solution at $\Gamma=7000$. The solid line is the numerical SMSA solution $h(r)$ and the dashed line is what one obtains by adding the leading-order to the next-to-leading order pole contribution, i.e.,

$$h^a(r)\equiv 2|\tilde{A}|\frac{e^{-\tilde{\alpha}_0 r}}{r}\cos(\alpha_1 r-\theta)+2|\overline{A}|\frac{e^{-\overline{\alpha}_0 r}}{r}\cos(\overline{\alpha}_1 r-\overline{\theta}). \tag{49}$$

The two conjugate pairs of complex poles and their amplitudes and phases were computed following Sec. II B 2, and their parameters are listed in Table II. The agreement between $h(r)$ and Eq. (49) suggests that, at least in the SMSA, the next-to-leading-order pole contribution does become important at intermediate distances in the very strong coupling regime and that the splitting of the second peak is due primarily to such contribution. Higher-order poles do contribute at $\Gamma=7000$ but are less important.

In the HNC, $\overline{h}(r)$ should decay as Eq. (48) provided $\overline{\alpha}_0 < 2\tilde{\alpha}_0$. Should this not be the case, then the contribution associated with the logarithmic branch point singularities should dominate over the next-to-leading-order pole contribution. In such circumstances we expect $\overline{h}(r)$ to decay [see Eq. (22)] as

$$\overline{h}(r) \propto 2|\tilde{A}|^2 \frac{e^{-2\tilde{\alpha}_0 r}}{r^2 \ln^2 r} \cos(2\alpha_1 r - 2\theta), \quad r \to \infty, \qquad (50)$$

where we have used the proportional sign to indicate that an additional prefactor will arise from the function $F(r)$ in Eq. (21). We have computed $\overline{h}(r)$ in the SMSA and HNC, at $\Gamma=100$, by subtracting the leading asymptotic contribution from the numerical result for $h(r)$. The results are plotted in Figs. 5(a) and 5(b) (solid lines). We note that the height of the first maximum of $\overline{h}(r)$ (near $2.5a_{\mathrm{WS}}$) for the SMSA in Fig. 5(a) is about 50% of that found for the HNC in Fig. 5(b). The leading-order pair of poles and their respective amplitudes and phases are listed in Table II.

Figure 5(a) shows there is very good agreement between $\overline{h}(r)$ and the decay given by Eq. (48), the next-to-leading-order pole contribution, with the parameters listed in Table II. This is not surprising since for the SMSA at $\Gamma=100$ the higher poles have much larger imaginary parts.

If we assume that in the strong coupling regime the HNC and SMSA poles should be similar, then for $\Gamma=100$ the imaginary part of the next-to-leading-order pole should satisfy $\overline{\alpha}_0 > 2\tilde{\alpha}_0$ and the decay of $\overline{h}(r)$ in the HNC should be determined by the logarithmic branch cut contribution, Eq. (50). The fact that we could not find any higher-order poles with imaginary part smaller than $2\tilde{\alpha}_0$ when solving Eqs. (25) and (26) numerically is consistent with this assumption. In Fig. 5(b) there is reasonable agreement between $\overline{h}(r)$ and the decay (50), the dashed line. The period of the oscillations is reproduced fairly well but $\overline{h}(r)$ decays less rapidly than is predicted by Eq. (50). Note that no attempt was made to adjust the amplitude. Although we feel that $\overline{h}(r)$ probably does reflect the presence of logarithmic branch singularities, it is very likely that the next-to-leading-order poles, which we are not able to calculate in the HNC (see Sec. III B), also make a substantial contribution in this range when $\Gamma=100$.

Accounting for the shoulder in the second peak of $h(r)$ at very high $\Gamma$ in the HNC is clearly more complicated than in the SMSA. We expect the next-to-leading-order pair of poles and the leading logarithmic singularities to contribute at intermediate range, i.e., we require Eq. (48) plus Eq. (50).

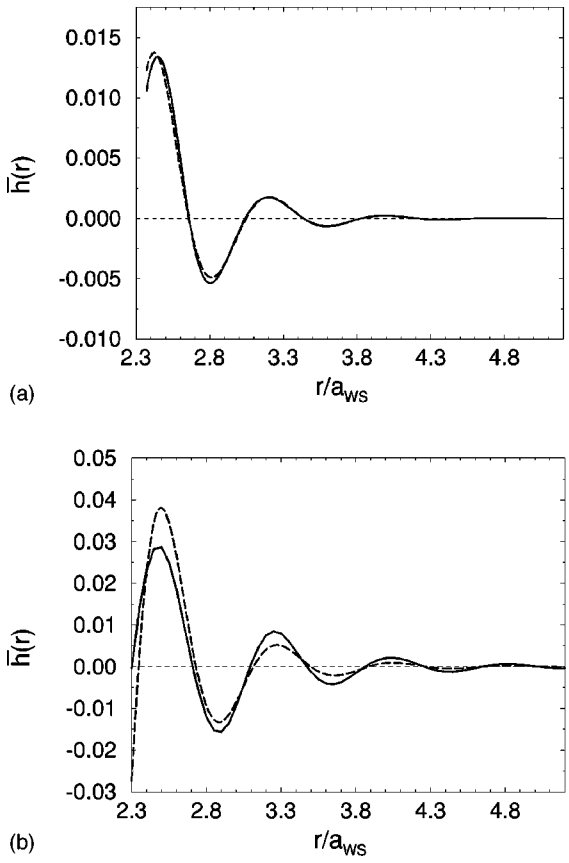


FIG. 5. The function $\overline{h}(r)$ defined by Eq. (47), i.e., $h(r)$ minus its leading asymptotic decay, for the OCP at $\Gamma=100$. (a) SMSA and (b) HNC. In both figures the solid line is obtained by subtracting the asymptotic contribution to $h(r)$, determined by the leading poles in Table II, from the solution to the integral equation. In (a) the dashed line is the contribution from the next-to-leading order pair of poles, Eq. (48), with the parameters given in Table II. In (b) the dashed line is the leading contribution from a logarithmic branch cut (50), with the parameters listed in Table II.

### D. Trajectories of poles

In order to understand the genesis of $h(r)$ and, indeed, thermodynamic properties of the OCP, it is necessary to determine the nature and location of the poles for the full range of $\Gamma$. In Fig. 6 we show the trajectories in the complex plane of seven poles of the OCP calculated in the SMSA. For $\Gamma < \Gamma_K = 2.1199$, there are two poles lying on the imaginary axis and an infinite number of complex poles. The leading pole is the pure imaginary pole closest to the real axis and for $\Gamma \ll 1$ this gives rise to Debye-Hückel-like limiting behavior. As $\Gamma$ is increased beyond $\Gamma_K$, the two imaginary poles merge and move off symmetrically into the complex plane while all other conjugate pairs of poles move down towards the real axis. Note that even at $\Gamma=7000$ the higher poles are still far from the real axis and the leading conjugate pair has $\tilde{\alpha}_0 = 0.0340$. According to the predictions of the general theory of the AHDL (Sec. II C), in the limit $\Gamma \to \infty$ all poles should touch the real axis at the points given by solutions of the equation $\alpha_1^{\infty} a_{\mathrm{WS}} = \tan(\alpha_1^{\infty} a_{\mathrm{WS}})$, and we have drawn the solid lines in Fig. 6 continuing to these points. We discuss the limiting behavior in the next subsection. It is instructive to compare the present results for the trajectories

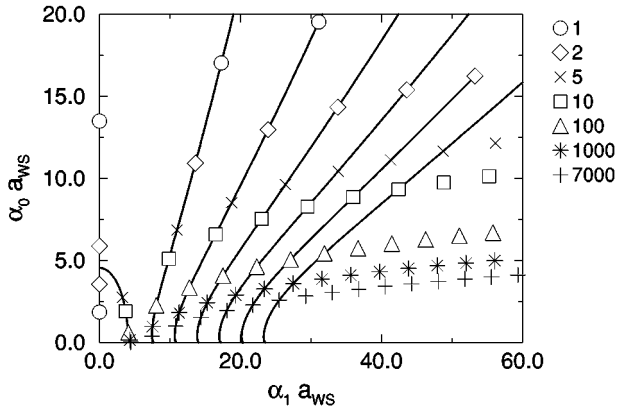


FIG. 6. Pole structure of the OCP treated in the SMSA at different values of $\Gamma$. The solid lines show the trajectories of the seven lowest poles as $\Gamma$ is varied up to $\Gamma=5\times10^7$. For $\Gamma=1,2$ there is a pair of poles lying on the imaginary axis. These merge as $\Gamma$ is increased towards $\Gamma_K=2.1199$ and then move off symmetrically into the complex plane. The plot shows only the right-hand complex poles $\alpha_1+i\alpha_0$. Note that the AHDL scaling relations (37)–(40) are obeyed accurately only when $\Gamma\approx10^7$.

in the OCP with those for the hard-sphere fluid, treated in the Percus-Yevick approximation for which $\hat{c}(q)$ is known analytically. Such a comparison is presented in Fig. 7, where the four lowest poles are shown. In the case of hard spheres there is no pole on the imaginary axis for any value of $\eta$. The two sets of trajectories are rather different. For hard spheres the real part $\alpha_1$ of each pole increases monotonically with increasing $\eta$, whereas for the OCP within the SMSA each $\alpha_1$ decreases with increasing $\Gamma$ (except for the leading-order pole) until very high values of $\Gamma$, when they reach a minimum value before finally increasing in the AHDL, i.e., $\Gamma\to\infty$.

### E. Results in the AHDL

The expected properties of the solutions of integral equations in the AHDL were described in Sec. II C. Here we

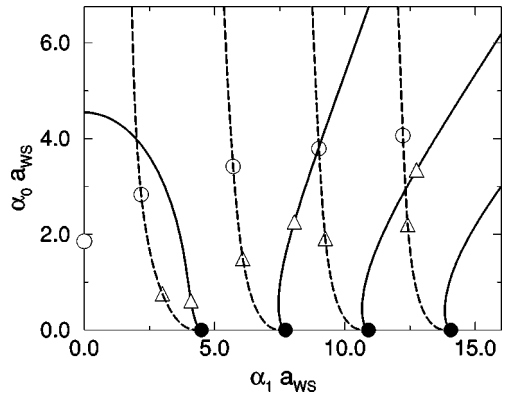


FIG. 7. The solid lines are the trajectories of the four lowest poles of the OCP treated in the SMSA at different $\Gamma$. The dashed lines are the four lowest poles of hard spheres treated in the PY approximation at different $\eta$ varied up to $\eta=0.95$. The open circles denote the poles at a fixed packing fraction $\eta=0.015\,79$ for the hard spheres and, on the imaginary axis, for the OCP with $\Gamma=1$. The triangles denote the poles at $\eta=0.2857$ which in the OCP corresponds to $\Gamma=100$. As $\Gamma\to\infty$ or $\eta\to1$, the poles meet the real axis at the solutions of $\alpha_1 a_{WS}=\tan(\alpha_1 a_{WS})$ represented by dots.

investigate the behavior of the potential energy, $c(r=0)$, and the poles of $\hat{h}(q)$ as the AHDL is approached, in both the HNC and SMSA. Within the SMSA we have generated the potential energy, $c(r=0)$, the poles, and their respective amplitudes as functions of $\Gamma$ using our own codes. For the potential energy in the HNC we use Ng's data [4] as well as our own, calculated from

$$\frac{\beta U}{N\Gamma}=\frac{3}{4\pi^2 a_{WS}^2}\int_0^\infty dq\ \hat{h}(q), \tag{51}$$

which was used also by Ng and which proves to be much more numerically reliable than the real-space counterpart (30). For $c(r=0)$ in the HNC we use our own data only, whereas for the leading poles in the HNC we employ Ng's data only, i.e., we assume that his least-squares fitting to Eq. (41) provides accurate parameters even for very large values of $\Gamma$, where we encountered difficulties with the direct calculation of the poles via Eqs. (25) and (26) because $c^{sr}(r)$ decays too slowly. In our HNC calculation we have used a mesh of 16 384 points with $\Delta r=0.0125$, whereas Ng used 2048 points for $\Gamma<600$ and 4096 otherwise, with $\Delta r=0.025$. Within the HNC, $\varepsilon$ is defined by [14]

$$\varepsilon=1-\eta\equiv1-(R/2a_{WS})^3, \tag{52}$$

where the effective diameter $R$ is the lowest value of $r$ for which $g(r)=1$, i.e., $g(r)<1$ for $r<R$. $R$ was determined numerically using a quadratic interpolation: $r(g(r))=a+bg(r)+cg^2(r)$, with three points, two for $g(r)<1$ and one for $g(r)>1$. The quadratic intersects the three points and $R\equiv r(1)=a+b+c$.

The results we present were obtained using Padé approximants [32] to extrapolate the desired quantities to the AHDL. Several sets of data in different ranges of $\Gamma$ were analyzed. The results we selected for publication are obtained from data at $\Gamma=200$, 250, 300, 350, 400, 500, 600, 800, 1000, 1200, 2000, 3000, 4000, 5000, and 6000, the same values as in Ng's paper [4]. Given the demanding numerical nature of this work, we believe it is useful to provide the actual data used in our calculations. These are compiled in Tables III and IV.

It is known that in the SMSA the AHDL analytical expansion for $\varepsilon$ in powers of $\Gamma$ is given by [33,14]

$$\varepsilon(\Gamma)=\left(\frac{108}{\Gamma}\right)^{1/6}-\frac{1}{3}\left(\frac{108}{\Gamma}\right)^{1/3}+\frac{5}{108}\left(\frac{108}{\Gamma}\right)^{1/2}-\frac{1}{243}\left(\frac{108}{\Gamma}\right)^{2/3}+\cdots. \tag{53}$$

This follows by solving Eq. (A9). In order to test our extrapolation scheme, we have computed the first and the second coefficients in this expansion by extrapolating first $\varepsilon\Gamma^{1/6}$ and second $[\varepsilon\Gamma^{1/6}-108^{1/6}]\Gamma^{1/6}$ as $1/\Gamma^{1/6}\to0$, using Padé approximants obtained from our numerical SMSA data. For the first coefficient we obtain $2.182\,247\,1\pm10^{-7}$, whereas $108^{1/6}=2.182\,247\,323$, and for the second we obtain $-1.587\,397\,4\pm10^{-7}$, whereas $-108^{1/3}/3=-1.587\,401\,126$.

TABLE III. Our present results for $c(r=0)$ and the potential energy $U$ of the OCP treated in both the SMSA and the HNC. Note that in the AHDL, $-c(r=0)/\Gamma=1.2$ and $-\beta U/N\Gamma=0.9$.

| | $-c(r=0)/\Gamma$ | | $-\beta U/N\Gamma$ | |
|---|---|---|---|---|
| $\Gamma$ | SMSA | HNC | SMSA | HNC |
| 200 | 1.218020 | 1.214319 | 0.87924043 | 0.87928 |
| 250 | 1.215787 | 1.213657 | 0.88145267 | 0.88165 |
| 300 | 1.214185 | 1.213142 | 0.88308323 | 0.88337 |
| 350 | 1.212968 | 1.212714 | 0.88434898 | 0.88470 |
| 400 | 1.212004 | 1.212342 | 0.88536827 | 0.88575 |
| 500 | 1.210562 | 1.211709 | 0.88692500 | 0.88735 |
| 600 | 1.209522 | 1.211174 | 0.88807266 | 0.88850 |
| 800 | 1.208097 | 1.210300 | 0.88896373 | 0.89009 |
| 1000 | 1.207149 | 1.209609 | 0.89077769 | 0.89114 |
| 1200 | 1.206461 | 1.209046 | 0.89158608 | 0.89192 |
| 1500 | 1.205714 | 1.208375 | 0.89247936 | 0.89276 |
| 2000 | 1.204883 | 1.207556 | 0.89349209 | 0.89370 |
| 3000 | 1.203921 | 1.206508 | 0.89469165 | 0.89481 |
| 4000 | 1.203361 | 1.205834 | 0.89540577 | 0.89545 |
| 5000 | 1.202983 | 1.205344 | 0.89589267 | 0.89587 |
| 6000 | 1.202708 | 1.204961 | 0.89625185 | 0.89621 |

TABLE IV. The parameter $\varepsilon\equiv 1-\eta(\Gamma)$ and the leading conjugate pair of complex poles with its amplitude $|\tilde{A}|$ obtained for the OCP in the SMSA. Note that in the AHDL, $\alpha_0 a_{\rm WS}=0$, $\alpha_1 a_{\rm WS}=4.493\,409\,5$, and $2|\tilde{A}|/a_{\rm WS}=3.143\,971\,7$. Also given is $\varepsilon\equiv 1-(R/2a_{\rm WS})^3$ for the HNC.

| $\Gamma$ | $\varepsilon$(HNC) | $\varepsilon$(SMSA) | $\alpha_0 a_{\rm WS}$ | $\alpha_1 a_{\rm WS}$ | $2\|\tilde{A}\|/a_{\rm WS}$ |
|---|---|---|---|---|---|
| 200 | 0.5820 | 0.6620336112 | 0.4203516 | 4.156587 | 2.853307 |
| 250 | 0.5694 | 0.6453657075 | 0.3703520 | 4.176180 | 2.815392 |
| 300 | 0.5588 | 0.6318424513 | 0.3330929 | 4.191907 | 2.791197 |
| 350 | 0.5497 | 0.6204862492 | 0.3039496 | 4.205009 | 2.775094 |
| 400 | 0.5417 | 0.6107125712 | 0.2803584 | 4.216211 | 2.764137 |
| 500 | 0.5284 | 0.5945239987 | 0.2441666 | 4.234609 | 2.751532 |
| 600 | 0.5174 | 0.5814421722 | 0.2174176 | 4.249317 | 2.746074 |
| 800 | 0.5001 | 0.5610900035 | 0.1799764 | 4.271859 | 2.745275 |
| 1000 | 0.4868 | 0.5455653443 | 0.1546377 | 4.288714 | 2.750397 |
| 1200 | 0.4759 | 0.5330606143 | 0.1361413 | 4.302029 | 2.757766 |
| 1500 | 0.4627 | 0.5179859013 | 0.1159965 | 4.317716 | 2.770098 |
| 2000 | 0.4458 | 0.4989394946 | 0.0937150 | 4.336865 | 2.790352 |
| 3000 | 0.4224 | 0.4728686628 | 0.0684934 | 4.361619 | 2.824746 |
| 4000 | 0.4061 | 0.4549383501 | 0.0543527 | 4.377505 | 2.851558 |
| 5000 | 0.3938 | 0.4413620959 | 0.0452126 | 4.388844 | 2.872905 |
| 6000 | 0.3839 | 0.4304871158 | 0.0387846 | 4.397472 | 2.890357 |

This exercise clearly shows that the accuracy of our Padé scheme is indeed quite high. The error listed for the extrapolated values is an estimation of the accuracy of the Padé scheme and is returned by the numerical routine used [32], rounded off to the nearest power of 10.

We carried out the calculation using our HNC data and obtained $1.847\pm 10^{-3}$ for the first coefficient in the expansion. There is no reason to expect a value identical to that found in the SMSA. Using the Padé approximants scheme for $1/\Gamma\to 0$, we obtain the following results:

| | SMSA | HNC—our data | HNC—Ng's data |
|---|---|---|---|
| $-\beta U/N\Gamma$ | $0.9000000\pm 10^{-7}$ | $0.8993\pm 10^{-4}$ | $0.9009\pm 10^{-4}$ |
| $-c(r=0)/\Gamma$ | $1.20034\pm 10^{-5}$ | $1.2007\pm 10^{-4}$ | |

We note that our treatment of Ng's potential energy data has produced a somewhat different result from his own, which gave $\beta U/N\Gamma=-0.8995\pm 0.0002$ [4]. The analytical AHDL expansion for the potential energy in the SMSA is known [33,14],

$$\beta\frac{U}{N}=-\frac{9}{10}\Gamma+3\left(\frac{\Gamma}{108}\right)^{1/2}+\frac{1}{15}\left(\frac{\Gamma}{108}\right)^{1/6}+O(\Gamma^{-1/6}). \tag{54}$$

We used Padé approximants to estimate the second coefficient in this expansion by considering our numerical results for $\Gamma^{-1/2}(\beta U/N)+0.9\Gamma^{1/2}$ in the limit $1/\Gamma^{1/3}\to 0$ and we find that the coefficient is

$$0.288\,675\,11\pm 10^{-8} \quad \text{whereas} \quad 3/108^{1/2}=0.288\,675\,134\,6.$$

Once again this attests to the reliability of the Padé scheme.

If we perform the same calculation using our own HNC data we obtain the value $0.28\pm 10^{-2}$ for this coefficient, while if we use Ng's data we obtain $0.25\pm 10^{-1}$. There is no obvious reason to expect the result to be the same as in the SMSA.

Finally, we have investigated the scaling relations for the leading poles. We extrapolated the values of $\tilde{\alpha}_0$ with $\varepsilon^6\to 0$ and of $\alpha_1$ and $|\tilde{A}|$ with $\varepsilon^3\to 0$ [see Eqs. (37)–(40)]. The results obtained from our SMSA data and from Ng's HNC data (Table III in [4]) are displayed in Table V. The amplitudes in these scaling relations were also computed and are listed in Table VI. $A_{\tilde{\alpha}_0}$ was computed by extrapolating the value of the ratio $\alpha_0 a_{\rm WS}/\varepsilon^6$ with $\varepsilon^6\to 0$. For $A_{\alpha_1}$ and $A_{\tilde{A}}$ we extrapolated, respectively, $(\alpha_1-\alpha_1^{\infty})a_{\rm WS}/\varepsilon^3$ and $2(|\tilde{A}|-|\tilde{A}^{\infty}|)/\varepsilon^3 a_{\rm WS}$, with $\varepsilon^3\to 0$.

The numerical estimates from the SMSA of the universal quantities $\alpha_0^{\infty}$, $\alpha_1^{\infty}$, and $|\tilde{A}^{\infty}|$ are in good agreement with the analytical results. The HNC estimates have larger error bars but these are also consistent with the predictions of the scaling relations (37)–(40). Note that the amplitudes (Table VI) do differ considerably between the two theories. We empha-

TABLE V. The analytical predictions and our numerical estimates from the SMSA and HNC for the leading conjugate pair of complex poles and its respective amplitude $|\tilde{A}^{\infty}|$ in the AHDL. The SMSA estimates were obtained by applying Padé approximants to the data in Table IV whereas the HNC estimates were obtained using data in Table III of [4] for the poles and amplitudes, and $\varepsilon(\Gamma)$ from our Table IV.

| | Analytical | SMSA | HNC |
|---|---|---|---|
| $\tilde{\alpha}_0^{\infty} a_{\mathrm{WS}}$ | 0 | $-0.00028 \pm 10^{-5}$ | $-0.011 \pm 10^{-3}$ |
| $\alpha_1^{\infty} a_{\mathrm{WS}}$ | 4.493409458 | $4.4939 \pm 10^{-4}$ | $4.50 \pm 10^{-2}$ |
| $2\lvert\tilde{A}^{\infty}\rvert / a_{\mathrm{WS}}$ | 3.14397174 | $3.1455 \pm 10^{-4}$ | $3.17 \pm 10^{-2}$ |

size that the Padé analysis for the SMSA and HNC was made using data for the same values of $\Gamma$, namely the values given previously and listed in Tables III and IV. Whereas there is no difficulty in solving the SMSA for arbitrarily large $\Gamma$, this is not the case for the HNC and like Ng [4] we did encounter problems for $\Gamma \gtrsim 7000$. The difference in error estimates reflects the fact that the SMSA is (essentially) an analytical theory whereas the HNC requires the numerical solution of a nonlinear integral equation.

We did not investigate the AHDL for higher poles as these could not be calculated within the HNC. However, they were calculated in the SMSA. One requires very large values, $\Gamma \sim 10^7$, before the appropriate scaling relations can be assumed to be valid and we did not check the generalization of Eqs. (37) and (38).

## IV. CONCLUDING REMARKS

We have presented a comprehensive analysis of the decay of correlations in the OCP. The main conclusions of our study are as follows.

(i) The mechanism for the onset of oscillations in $h(r)$ in the OCP is the same as that for *charge* correlations in the RPM or the YRPM. It arises from the coalescence of two imaginary poles, which exist for $\Gamma < \Gamma_K$, to produce a conjugate pair of complex poles for $\Gamma > \Gamma_K$. At the crossover value $\Gamma_K$ the wavelength of the oscillations is infinite. We obtain values for $\Gamma_K$ equal to 2.1199 and 1.120 in the SMSA and the HNC, respectively. It is important to recognize that this mechanism is very different from that found for the onset of oscillations in simple fluids where the interatomic potential exhibits (short-ranged) attraction as well as repulsion. There [8,9,11] a single imaginary pole dominates at low density whereas a conjugate complex pair dominates at high density. At the crossover point (termed the Fisher-Widom [34] value) the imaginary pole and the conjugate pair have the same imaginary part, $\alpha_0 = \tilde{\alpha}_0 \neq 0$, and the wavelength of the oscillations is finite. Such crossover results from a competition between repulsive and attractive forces.

(ii) In both the monotonic, $\Gamma < \Gamma_K$, and oscillatory, $\Gamma > \Gamma_K$, regimes, leading-order asymptotics provide a remarkably accurate description of $h(r)$ at intermediate as well as long range. This is due to the fact that, as in other fluids [8,11,10,24], the leading pole(s) are well-separated from the remaining poles or singularities.

(iii) In the SMSA, where we are able to calculate all the poles, we showed that the contribution from the next-to-leading conjugate pair of poles leads to a splitting of the second maximum in $h(r)$ when $\Gamma \gtrsim 2000$. Determining the higher-order poles in the HNC by direct calculation is not possible if these have an imaginary part greater than $2\tilde{\alpha}_0$. Attempts at fitting the next-to-leading-order decay of $h(r)$ to particular asymptotic forms in order to determine the higher-order poles are also problematic since, within the HNC, contributions from logarithmic branch points are expected to intervene. What the *actual* next-to-leading-order decay of $h(r)$ is for the OCP remains to be ascertained. An excellent fit to simulation data for $h(r)$ beyond the first maximum was obtained by assuming it was the sum of three terms with the form (45) [35] but this does not prove that there are only pole contributions.

TABLE VI. The amplitudes in the scaling relations (37)–(40) for the poles of the OCP in the AHDL. The results for the SMSA were obtained by applying Padé approximants on our own generated data. The results for the HNC were computed using the parameters in Table III of [4] for the leading poles and our own data in Table IV for $\varepsilon(\Gamma)$.

| | SMSA | HNC |
|---|---|---|
| $A_{\tilde{\alpha}_0}$ | $4.48 \pm 10^{-2}$ | $15 \pm 1$ |
| $A_{\alpha_1}$ | $0.64 \pm 10^{-2}$ | $1.787 \pm 10^{-3}$ |
| $A_{\tilde{A}}$ | $-1.8 \pm 10^{-1}$ | $-1.67 \pm 10^{-2}$ |

(iv) Our investigation of the AHDL of the OCP has amplified that of Ref. [14]. Within the SMSA there is, of course, no difficulty in obtaining the solutions, poles, etc. with arbitrary precision and all the predictions associated with the AHDL have been confirmed. The present work demonstrates that the asymptotic regime is not entered until $\Gamma$ is very high indeed—see Fig. 6. Even for $\Gamma$ as high as 7000, the trajectories of the higher poles have not attained behavior which resembles remotely that of the AHDL. The situation is much better for the leading pole, which is why we were able to conduct the Padé analysis based on data for $\Gamma \leqslant 6000$. Although the numerical solutions of the HNC are less accurate than the input from the SMSA, our analysis does suggest that the predictions of the AHDL are also obeyed by the HNC—at least for the quantities $c(r=0)/\Gamma$, $\beta U/N$, and the parameters of the leading pole which we were able to calculate. We provide new estimates for the various coefficients entering the expansions of the quantities.

(v) While our results support the ideas of universality of structure conjectured for the AHDL, and therefore support the description of the limit $\eta = 1$ as defining an *ideal* liquid, it is clear from Figs. 6 and 7 that one soon leaves the AHDL. This is confirmed by plotting the results on an expanded scale for large $\eta$. Whether one can use predictions based on the AHDL to describe the properties of stable (with respect to the solid) dense liquids remains a matter for further investigation and debate.

As a final remark we mention that our analysis also has implications for the decay of (one-body) density profiles at wall-fluid interfaces. It is straightforward to show [8,9,36] that the profile at a single wall and the solvation force for a confined fluid decay into bulk in the same fashion as $h(r)$, i.e., with the same exponential decay length $\alpha_0^{-1}$ and, when

appropriate, the same oscillatory wavelength $\alpha_1^{-1}$. Only the amplitudes and phases depend on the particular form of the wall-fluid potentials—note the latter must be short-ranged. These results are a consequence of the fact that for fluids with short-ranged interatomic potentials the asymptotic decay of the profile and the solvation force is governed by the leading poles of the bulk function $\hat{h}(q)$. We expect the same results to be valid for the OCP subject to external potentials, e.g., a hard-wall or a half-space of compensating charge background. Thus, for $\Gamma<\Gamma_K$ we predict monotonic decay and for $\Gamma>\Gamma_K$ oscillatory decay of the density profile into bulk. The wavelength should decrease and the decay length of the oscillations should increase as $\Gamma$ is increased. Although there have been several theoretical and simulation studies of the OCP near walls [37], these have not addressed the predictions we give here.


## ACKNOWLEDGMENTS

R.J.F.L.d.C. thanks JNICT/PRAXIS XXI (Portugal) for financial support during his studies in Bristol. He is presently carrying out work at the ENS de Lyon as part of a project financed by the European Commission through the Training and Mobility of Researchers (TMR) Programme. We are grateful to Thierry Biben for his valuable comments about the numerical methods.


## APPENDIX A: THE OCP TREATED IN THE SMSA

We consider a system of charged hard spheres of diameter $d$ immersed in a uniform oppositely charged background which preserves the overall electrical neutrality. The interionic potential is

$$\begin{aligned}\beta\phi(r)&=\infty, \quad r<d\\ &=\beta\frac{e^2}{r}, \quad r>d.\end{aligned} \tag{A1}$$

The MSA for this system consists of the Ornstein-Zernike relation (3), the exact condition due to the hard-core $h(r)=-1$ for $r<d$, and the closure approximation $c^{sr}(r)\equiv c(r)+\beta\phi(r)=0$ for $r>d$. The solution to the MSA for this problem was given by Palmer and Weeks [38] and reads

$$\begin{aligned}c(x)=A+6\eta M^2x+\frac{1}{6}\kappa^2x^2\\ +\frac{1}{2}\eta(A+\kappa^2V)x^3+\frac{\eta\kappa^2}{60}x^5, \quad x<1,\end{aligned} \tag{A2}$$

where $x\equiv r/d$ and the dimensionless coefficients are determined by the following equations:

$$A=-\frac{(1+2\eta)^2}{(1-\eta)^4}+\frac{Q^2}{4(1-\eta)^2}-\frac{(1+\eta)Q\kappa}{12\eta}-\frac{(5+\eta^2)\kappa^2}{60\eta}, \tag{A3}$$

$$V=-\frac{(1+\eta-\eta^2/5)}{12\eta}-\frac{(1-\eta)Q}{12\eta\kappa}, \tag{A4}$$

$$Q=\frac{1+2\eta}{1-\eta}\left[1-\left(1+\frac{2(1-\eta)^3\kappa}{(1+2\eta)^2}\right)^{1/2}\right], \tag{A5}$$

$$M=\frac{Q^2}{24\eta}-\frac{1+\eta/2}{(1-\eta)^2}, \tag{A6}$$

$\eta$ is the packing fraction and $\kappa^2=\kappa_D^2d^2=4\pi\beta\rho e^2d^2=12\Gamma\eta^{2/3}$. Note that the parameter $V$ is proportional to the potential energy $U$,

$$\frac{\beta U}{N}=\frac{1}{2}\kappa^2V. \tag{A7}$$

The continuity of $h(x)-c(x)$ at $x=1$ requires

$$g(x=1^+)=-M=-c^{sr}(x=1^-). \tag{A8}$$

In the SMSA for a soft potential one imposes an additional condition to the MSA closure, i.e., the continuity of the pair distribution function at the hard-sphere diameter. Thus the effective diameter $R$ is chosen so as to ensure that $g(r)$ is always continuous and $g(x=1^+)=0$. From Eq. (A8) this implies $M\equiv0$. In practice, for the OCP at a given $\Gamma$ the packing fraction $\eta\equiv\eta(\Gamma)=\rho\pi R^3/6$ is chosen so that the condition $M=0$ is satisfied. It follows that $\eta(\Gamma)$ satisfies

$$\begin{aligned}0=2(6\eta+3\eta^2)^{1/2}+1+2\eta\\ -[(1+2\eta)^2+4(1-\eta)^3\eta^{1/3}\sqrt{3\Gamma}]^{1/2}\end{aligned} \tag{A9}$$

which can be solved numerically for $\eta(\Gamma)$ using a Newton-Raphson procedure.

## APPENDIX B: AMPLITUDE AND PHASE FOR SIMPLE POLE CONTRIBUTIONS IN THE OCP

In this appendix we describe the evaluation of the amplitude and phase of contributions to $h(r)$ arising from simple poles. It is assumed that $c^{sr}(r)$ has been obtained numerically from the HNC or another closure approximation.

If a pure imaginary pole, $q=i\alpha_0$, is found by solving Eq. (28), then its amplitude in the expansion (15) of $h(r)$ is given by

$$A=-\frac{1}{2\pi\rho^2}\frac{i\alpha_0}{d\hat{c}(i\alpha_0)/di\alpha_0}, \tag{B1}$$

where the derivative of $\hat{c}(q)$ can be obtained from Eq. (24) and is given by

$$\begin{aligned}\frac{d\hat{c}(i\alpha_0)}{d\alpha_0}=\frac{4\pi}{\alpha_0}\int_0^\infty dr\ rc^{sr}(r)\left[r\cosh(\alpha_0r)-\frac{\sinh(\alpha_0r)}{\alpha_0}\right]\\ -\frac{2}{\alpha_0\rho}\left(\frac{\kappa_D}{\alpha_0}\right)^2.\end{aligned} \tag{B2}$$

Consider now a conjugate pair of complex poles $q=\pm\alpha_1+i\tilde{\alpha}_0$. Using Eq. (10) in Eq. (15) leads to the following expression for the amplitude of the contribution of a single complex pole:

$$A=-\frac{1}{2\pi\rho}\left[\frac{q}{\rho d\hat{c}^{sr}(q)/dq+2\kappa_D^2/q^3}\right]. \tag{B3}$$

It is useful to introduce the functions $a$ and $b$ defined by

$$\hat{c}^{sr}(q)\equiv\frac{4\pi}{q}(a-ib) \tag{B4}$$

and the functions $c$ and $d$ defined by

$$\frac{d\hat{c}^{sr}(q)/dq}{q}\equiv-\frac{1}{q^2}[\hat{c}^{sr}(q)-4\pi(c-id)]. \tag{B5}$$

Then, for the positive pole $q\equiv+\alpha_1+i\tilde{\alpha}_0$, it follows that

$$\begin{aligned} a&=\int_0^\infty dr\, rc^{sr}(r)\sinh(\tilde{\alpha}_0 r)\cos(\alpha_1 r),\\ b&=\int_0^\infty dr\, rc^{sr}(r)\cosh(\tilde{\alpha}_0 r)\sin(\alpha_1 r) \end{aligned} \tag{B6}$$

and

$$\begin{aligned} c&=\int_0^\infty dr\, r^2c^{sr}(r)\cosh(\tilde{\alpha}_0 r)\cos(\alpha_1 r),\\ d&=\int_0^\infty dr\, r^2c^{sr}(r)\sinh(\tilde{\alpha}_0 r)\sin(\alpha_1 r). \end{aligned} \tag{B7}$$

The (complex) amplitude of this pole, $A^+\equiv|\tilde{A}|e^{-i\theta}$ [see the discussion after Eq. (17)], can be written as

$$\begin{aligned} |\tilde{A}|^{-1}e^{i\theta}&=-\frac{2\pi\rho}{q}\left[\frac{\rho d\hat{c}^{sr}(q)}{dq}+2\frac{\kappa_D^2}{q^3}\right]\\ &=\frac{8\pi^2\rho^2}{q^2}\left[\frac{a-ib}{\tilde{\alpha}_0-i\alpha_1}-(c-id)-(f-ig)\right]\\ &=\frac{8\pi^2\rho^2}{q^2}(\tilde{a}+i\tilde{b}), \end{aligned} \tag{B8}$$

where

$$f-ig\equiv\kappa_D^2/(2\pi\rho q^2) \tag{B9}$$

and

$$\tilde{a}=\frac{a\tilde{\alpha}_0+b\alpha_1}{\tilde{\alpha}_0^2+\alpha_1^2}-c-f,\quad \tilde{b}=\frac{a\alpha_1-b\tilde{\alpha}_0}{\tilde{\alpha}_0^2+\alpha_1^2}+d+g. \tag{B10}$$

Rearranging Eq. (B8), we obtain

$$|\tilde{A}|e^{-i\theta}=\frac{(\tilde{\alpha}_0^2+\alpha_1^2)}{8\pi^2\rho^2\sqrt{\tilde{a}^2+\tilde{b}^2}}e^{-i(t-2p)} \tag{B11}$$

with the angles $p$ and $t$ determined by

$$e^{ip}=\frac{\alpha_1+i\tilde{\alpha}_0}{\sqrt{\tilde{\alpha}_0^2+\alpha_1^2}}\quad e^{it}=\frac{\tilde{a}+i\tilde{b}}{\sqrt{\tilde{a}^2+\tilde{b}^2}}. \tag{B12}$$

Using Eq. (B9), it follows that

$$f=\frac{\kappa_D^2}{2\pi\rho}\frac{\alpha_1^2-\tilde{\alpha}_0^2}{(\tilde{\alpha}_0^2+\alpha_1^2)^2},\quad g=\frac{\kappa_D^2}{2\pi\rho}\frac{2\alpha_1\tilde{\alpha}_0}{(\tilde{\alpha}_0^2+\alpha_1^2)^2}. \tag{B13}$$

In order to compute the amplitude and phase of a conjugate pair of complex poles $q=\pm\alpha_1+i\tilde{\alpha}_0$ we employ $c^{sr}(r)$ in Eqs. (B6) and (B7) to find $a$, $b$, $c$, and $d$. Then $\tilde{a}$ and $\tilde{b}$ are evaluated from Eq. (B10) with Eq. (B13). Finally we use these results in Eq. (B11) to find $|\tilde{A}|$ and the phase $\theta=t-2p$, with the angles $t$ and $p$ calculated from Eq. (B12). Note that the range of convergence of the integrals in Eqs. (B6) and (B7) is the same as in Eqs. (25) and (26) and this prescription for determining the amplitudes and phases is only valid provided the poles themselves can be determined from the latter pair of equations.


[1] See, e.g., M. Baus and J.-P. Hansen, Phys. Rep. **59**, 1 (1980); S Ichimaru, Rev. Mod. Phys. **54**, 1017 (1982).

[2] See, e.g., J.-P. Hansen and I. R. McDonald, *Theory of Simple Liquids* (Academic Press, London, 1986).

[3] J. F. Springer, M. A. Pokrant, and F. A. Stevens, Jr., J. Chem. Phys. **58**, 4863 (1973).

[4] K.-C. Ng, J. Chem. Phys. **61**, 2680 (1974).

[5] Y. Rosenfeld and N. W. Ashcroft, Phys. Rev. A **20**, 1208 (1979).

[6] W. L. Slattery, G. D. Doolen, and H. E. DeWitt, Phys. Rev. A **21**, 2087 (1980).

[7] J.-P. Hansen, Phys. Rev. A **8**, 3096 (1973); E. L. Pollock and J.-P. Hansen, *ibid.* **8**, 3110 (1973).

[8] R. Evans, R. J. F. Leote de Carvalho, J. R. Henderson, and D. C. Hoyle, J. Chem. Phys. **100**, 591 (1994).

[9] R. Evans and R. J. F. Leote de Carvalho, in *Chemical Applications of Density-Functional Theory*, edited by B. B. Laird, R. B. Ross, and T. Ziegler, ACS Symposium Series 629 (American Chemical Society, Washington, DC, 1996), p. 166.

[10] R. J. F. Leote de Carvalho and R. Evans, Mol. Phys. **83**, 619 (1994).

[11] R. J. F. Leote de Carvalho, R. Evans, D. C. Hoyle, and J. R. Henderson, J. Phys.: Condens. Matter **6**, 9275 (1994).

[12] Y. Rosenfeld and N. W. Ashcroft, Phys. Rev. A **20**, 2162 (1979), and references therein.

[13] Y. Rosenfeld, J. Stat. Phys. **37**, 215 (1984).

[14] Y. Rosenfeld, Phys. Rev. A **33**, 2025 (1986).

[15] Y. Rosenfeld, Phys. Rev. A **32**, 1834 (1985); **37**, 3403 (1988);

see also the review Y. Rosenfeld, in *The Equation of State in Astrophysics*, edited by G. Chabrier and E. Schatzman (Cambridge University Press, Cambridge, 1994), p. 78.
[16] J. G. Kirkwood, Chem. Rev. **19**, 275 (1936).
[17] R. Kjellander and D. J. Mitchell, J. Chem. Phys. **101**, 603 (1994); J. Ennis, R. Kjellander, and D. J. Mitchell, *ibid.* **102**, 975 (1995).
[18] M. J. Gillan, Mol. Phys. **38**, 1781 (1979).
[19] P. Attard, Phys. Rev. E **48**, 3604 (1993).
[20] G. A. Martynov and G. N. Sarkisov, J. Chem. Phys. **93**, 3445 (1990).
[21] G. A. Martynov, *Fundamental Theory of Liquids: Method of Distribution Functions* (Adam Hilger, Bristol, 1992), Sec. 5.5.
[22] C. Vega, L. F. Rull, and S. Lago, Phys. Rev. E **51**, 3146 (1995).
[23] S. G. Brush, H. L. Sahlin, and E. Teller, J. Chem. Phys. **45**, 2102 (1966).
[24] R. J. F. Leote de Carvalho and R. Evans, Mol. Phys. **92**, 211 (1997).
[25] Ph. Choquard and R. R. Sari, Phys. Lett. **40A**, 109 (1972).
[26] F. Del-Rio and H. E. DeWitt, Phys. Fluids **12**, 791 (1969).
[27] M. S. Cooper, Phys. Rev. A **7**, 1 (1973).
[28] C. Deutsch, Y. Furutani, and M. Gombert, Phys. Rev. A **13**, 2244 (1976).
[29] W. E. Brown, R. J. F. Leote de Carvalho, and R. Evans, Mol. Phys. **88**, 579 (1996).
[30] E. Waisman, Mol. Phys. **25**, 45 (1973).
[31] G. Stell and S. F. Sun, J. Chem. Phys. **63**, 5333 (1975); J. S. Høye and G. Stell, Mol. Phys. **32**, 195 (1976).
[32] W. H. Press, S. A. Teukolsky, W. T. Vetterling, and B. P. Flannery, *Numerical Recipes: The Art of Scientific Computing* (Cambridge University Press, Cambridge, 1992).
[33] D. MacGowan, J. Phys. C **16**, 59 (1983).
[34] M. E. Fisher and B. Widom, J. Chem. Phys. **50**, 3756 (1969).
[35] D. M. Ceperley and G. V. Chester, Phys. Rev. A **15**, 755 (1977).
[36] R. Evans, J. R. Henderson, D. C. Hoyle, A. O. Parry, and Z. A. Sabeur, Mol. Phys. **80**, 755 (1993).
[37] See Figure 18 and Refs. [55,56] of Y. Rosenfeld, J. Chem. Phys. **98**, 8126 (1993).
[38] R. G. Palmer and J. D. Weeks, J. Chem. Phys. **58**, 4171 (1973).